

Numerical study of pipeline leak detection for gas-liquid stratified flow

Mutiu Adesina Adegboye^a, Aditya Karnik ^{a*}, Wai-Keung Fung^{a,b}

^aSchool of Engineering, Robert Gordon University, Aberdeen AB10 7GJ, UK

^bDepartment of Applied Computing and Engineering, Cardiff School of Technologies, Cardiff Metropolitan University, Llandaff Campus, Western Avenue, Cardiff, CF5 2YB, UK

*Corresponding author; Tel: +44 (0)1224 263335, E-mail address: a.karnik@rgu.ac.uk

Abstract

Multiphase flows are of paramount importance in the oil and gas industry, considering that most petroleum industries produce and transport oil and gas simultaneously. However, systematic research on pipeline leakage conveying more than one phase at a time is lacking attention. In this work, a numerical method is proposed to investigate the effect of two-phase gas-liquid leak flow behaviour in a subsea natural gas pipeline. The results of the simulations have been validated against the latest experimental and numerical data reported in the literature, and a good agreement has been obtained. The effect of leak sizes, longitudinal leak locations, multiple leakages and axial leak positions on the pressure gradient, flow rate and volume fractions in the pipeline were systematically investigated. The results show that the flow field parameters provide pertinent indicators in pipeline leakage detection. In particular, the upstream pipeline pressure could serve as a critical indicator for detecting leakage even if the leak size is small. Whereas, the downstream flow rate is a dominant leakage indicator if the flow rate monitoring is

chosen for leak detection. The results also reveal that when two leaks with different sizes co-occur in a single pipe, detecting the small leak becomes difficult if its size is below 25% of the large leak size. However, in the event of a double leak with equal sizes, the leak closer to the pipe upstream is easier to detect.

Keywords: Loss prevention; Multiphase flow; Natural gas transportation; Numerical simulation; Pipeline leak detection.

1. Introduction

Pipelines are one of the primary tools in the oil and gas industry, which play a unique role in the process of gathering and delivering petroleum, hydrocarbon exploration and transportation (Sun *et al.*, 2019; Wang *et al.*, 2021). The use of pipelines has extended over time because it provides an effective system to increase energy supply and has been considered the safest and the most economical and efficient means of petroleum transportation (Muggleton *et al.*, 2020). For example, the average estimated deaths due to accidents per ton-mile of shipped petroleum products using trucks, ships and rails are respectively 87%, 4% and 2.7% more than those using pipelines (Cramer *et al.*, 2015; Adegboye *et al.*, 2019). However, a leak in pipeline remains a major concern for both safety and contamination in the environment (Li *et al.*, 2019a) in daily operation, and the likelihood of developing leaks increases with the ages and service time of the pipeline (Li *et al.*, 2018; Mohammed *et al.*, 2019). Different factors that are accountable for pipeline leakage include corrosion, defects during installation and erection work (Bolotina *et al.*, 2018).

A leak in subsea pipelines creates a serious problem in maintaining safe, reliable, and effective offshore production facilities (Li *et al.*, 2019b). Unlike leak on surface or water transportation

pipeline, which are also of great concern. A leak in a subsea pipeline always puts the marine environment at risk. It also causes devastating disasters, resulting in assets damage, environmental pollution, human casualties, and corporate reputation loss (Ajao *et al.*, 2018). Besides the harmful effect of submarine pipeline leakage on the aquatic animals, subsea pipeline leak often causes oil spills into the sea region, making the detection and diagnosis difficult (Li *et al.*, 2019b). Thereby, it costs a significant amount of money and time to clean up the contaminated regions (Wei and Masuri, 2019).

Several safety regulations include the safety (PIPES) Act of 2006 and 2016 in the USA (Scott and Scott, 2019), the United States of energy policy and safety regulation (Scott, 2018), British Standard BS 8010 (Movley, 2005), among others have been established to ensure safe pipeline operations (Kazeem *et al.*, 2017; Ijaola *et al.*, 2020). Despite stricter regulations and maintenance practice imposed by different governments, several pipeline leakages are often reported worldwide (Dasgupta, 2016; Joling, 2017). The amounts of resources lost to these incidents are enormous (Wei and Masuri, 2019). To reduce the effects of accidental pipeline leakage, it is paramount to monitor pipelines for timely and accurate leak detection. The early leak detection will aid quick response to seize petroleum discharge and mitigate associated risks such as fire, explosion and system downtime, and thus will extend the petroleum transportation facilities lifetime.

2. Related Works

Several studies on pipeline leak detection methods have been proposed in the literature (Ben-Mansour *et al.*, 2012; Karim *et al.*, 2015; Wang and Ghidaoui, 2018; Syed *et al.*, 2020; Wang *et al.*, 2021). Existing leak detection and diagnostic are classified into software and hardware

approaches. In an effort to classify these technologies based on the technical nature, further research efforts were made and led to the classification into three groups, namely external, visual or biological and internal methods (Adegboye *et al.*, 2019). The external technologies utilise human-made sensing devices to achieve leak detection tasks at the exterior part of the pipeline. The visual-based methods employ experienced personnel, trained dogs, pigs and drones to inspect and detect pipeline leakage. This approach appears to be the most suitable for leak detection and localisation. However, the operational time of these techniques is based on the frequency of inspection. Readers are referred to Adegboye *et al.* (2019) for further details on the review of pipeline leakage detection methods.

Many researchers have reported a collection of techniques to detect and localise pipeline leakage for the internal-based leak detection methods. Generally, these methods employ computational algorithms in conjunction with various sensors for monitoring parameters that quantitatively characterise the fluid flow within pipelines. Some commonly used techniques include mass-volume balance (Karim *et al.*, 2015; Syed *et al.*, 2020), negative pressure wave (Elaoud *et al.*, 2010; Datta and Sarkar, 2016; Chen *et al.*, 2018), pressure point analysis (bin Md *et al.*, 2011), state estimator (Ali *et al.*, 2015, Chen *et al.*, 2021), and dynamic modelling (Yang *et al.*, 2010; Li *et al.*, 2019b). Among these methods, dynamic modelling, also known as real-time transient modelling, is the most sensitive method (Guerriero *et al.*, 2016; Liu *et al.*, 2019). This method employs conservation equations for the fluid mass, momentum and energy to model the flow within a pipeline and compares the predicted values with the measured data to determine and characterise leakages. The flow parameters monitored in this method are flow rate, pressure, and other fluid flow parameters. Pipeline leak detection using transient-based leak detection approach has been extensively adopted in the research community (Araújo *et al.*, 2013; Araújo *et al.*,

2014; Lazhar *et al.*, 2013; De Sousa and Romero, 2017; Fu *et al.*, 2020; Ranawat and Nandwana, 2021), and it has been shown to be successful in detecting and locating pipeline leak position. However, most of the work reported in the literature is limited to single-phase systems (Elaoud *et al.* 2010; Yang *et al.*, 2010; Lazhar *et al.*, 2013; Araújo *et al.* 2014; Ben-Mansour *et al.* 2012; De Sousa and Romero 2017; Li *et al.*, 2019; Wang *et al.*, 2021).

De Sousa and Romero (2017) investigated oil leak influence on the pressure and flow rate characteristics using ANSYS Fluent. The obtained results revealed how the leak impacted both pressure and flow rate within the leak region vicinity. Molina-Espinosa *et al.* (2013) carried out numerical modelling backed up by physical experiments for pipe leaks. In this study, transient modelling of incompressible flow in short pipes with leaks was investigated. The obtained results revealed good correlations between the simulation and experimental data in terms of pressure drop within the vicinity of the leakages.

A relevant study on subsea pipelines by Zhu *et al.* (2014) simulated oil released from submarine pipelines subjected to different leak sizes. In this study, the effects of oil leak rate, leak sizes, oil density and water velocity on the oil spill behaviour were investigated using the Volume of Fluid (VOF) method. This study revealed that small leak size, slow leaking and high fluid density led to a long period for oil to reach the maximum horizontal migrate distance. In a similar study by Li *et al.* (2018), a numerical investigation of submarine pipeline spillage was carried out using ANSYS Fluent to forecast oil spill trajectory movement. The quantity and trajectory of spilt oil under various operating pressure, current sea velocities and wavelengths were analysed.

Li *et al.* (2017) employed Computational Fluid Dynamics (CFD) models to describe underwater oil release rate and its trajectory movement from the damaged subsea pipeline to the free surface

of the water. The simulated results revealed that the developed model could provide a detailed understanding of pipeline leakage, such as gas release rate, horizontal dispersion distance and gas rising time in a subsea environment. However, gas movement trajectory behaviour can only be predicted in a shallow ocean as the sea wave can easily alter the leaking fluid dispersion movement. The approach to the subsea pipeline leakages reported in the literature (Zhu *et al.*, 2014; Li *et al.*, 2017; Singh *et al.*, 2017) shows that consideration of the impact of leaks on fluid flow parameters within the pipeline in a subsea environment is yet to be well understood.

The extensive review reveals that literature on a multiphase pipeline leakage is rather limited. Most of the available literature focuses on single-phase flow. Multiphase flow systems are generally encountered not only in the oil and gas industry, nuclear, chemical process industries, among others. As such, the development of an accurate leak prediction model is timely and essential as this will aid in advancing rapid pipeline leak detection technologies for these critical applications.

In the context of multiphase pipeline leak detection, the computational study by Kam (2010) investigated the influence of leak sizes and the longitudinal locations of the leak on flow parameters. However, this study was only limited to a 1-D pipeline, assuming that the pipeline was made up of a series of small segments in which each node along the pipe modelled the local flow characteristics. A similar study presented by Figueiredo *et al.* (2017) investigated the effect of leakage on two-phase flow behaviour in nearly horizontal pipelines. In their study, the impact of longitudinal leak location on stratified flows was investigated. The finding revealed that pressure profiles commonly employed in monophasic leakage's could be extended to the stratified flow system. The limitation of this work, however, restriction to a 1-D pipeline. The empirical

models do not adequately capture all the dynamics of the multiphase flow behaviour. These analytical solution assumptions restrict their capability to consider different scenarios in which leak may occur in 3-D pipelines.

The 3-D CFD modelling approach promises to be an effective tool to investigate complex multiphase flow problems (Singh *et al.*, 2017; Saeedipour *et al.*, 2019; Alghurabi *et al.*, 2021). It avoids unrealistic assumptions usually adopted in the empirical models for multiphase pipeline leakage. CFD models provide an opportunity to incorporate intricate pipeline configuration and offer detailed information of multiphase flow systems that may be difficult to obtain using analytical models or physical experiments. In particular, 3-D CFD models can readily investigate the influence of the radial position of the leak along the circumference of the pipe relative to the gas-liquid interface. Araújo *et al.* (2013) investigated leak influence in hydrodynamics of oil-water two-phase flow in a horizontal pipeline. The simulation was performed in ANSYS CFX using the Eulerian-Eulerian model by considering the oil as a continuous phase and water as a dispersed phase. The authors varied the volume fraction of oil at the inlet of the pipeline. They observed that the amount of oil discharged from the leak region reaches a stable value after around 0.4 s for all the simulations reported in their study. However, their study is limited to the leak effect before the flow stability time. Also, their study applicability may be limited since they did not report a particular flow pattern. Besides, the effects of radial and longitudinal leak locations, leak opening sizes and multiple leakages remain to be investigated. To better understand the fluid flow behaviour induced by leak for the aforementioned effects, the present study extends the multiphase pipeline leakage to both before and after the flow stability state.

This study motivation is the lack of research that systematically investigates pipeline leakage conveying more than one phase at a time. A number of studies have been carried out to understand monophasic pipeline leakages. However, not much is known regarding the multiphase pipeline system. A recent study by Behari *et al.* (2020) noted that the available leak detection techniques in the open literature fail to satisfactorily address multiphase pipeline leakage phenomena. There is no guarantee that the information available for single pipeline leak cases can be extended to multiphase pipeline system. This is evident that more insight into pipeline transporting more than one is needed to attain a thorough understanding of pipeline leakage in this context.

The present paper is primarily aimed at investigating accidental leakage of pipeline in a subsea environment as a multiphase flow system. Plausible leak scenarios which may occur in the field have been covered. A comprehensive assessment of different leak sizes, longitudinal leak locations, radial positions, and multiple leakages are performed for a gas-liquid pipeline using a 3-D CFD model. Specifically, RANS equations are model to study pipeline leakage. The perturbation of the pertinent flow field indicators for different leak scenarios is reported, which is expected to help in improving the understanding of multiphase flow behaviour induced by leaks. The simulation results are validated against the numerical simulation by Chinello et al. (2019) and experimental data reported in Espedal (1998). In particular, monophasic and stratified flow behaviours induced by leaks are compared and validated with the experimental data reported by Monina-Espinosa et al. (2013). This study will lead to developing an improved multiphase pipeline leak prediction system, providing guides for timely detection of multiphase pipeline leakage, and preventing injuries and damage to properties.

The rest of the paper is organised as follows: Section 3 presents the computational model used for analysis, while Section 4 gives details of the numerical method and parameters. Detailed simulation results will be analysed and discussed in Section 5. The summary and conclusion of the research findings, including the recommendations for further work, are presented in Section 6.

3. Computational model

In order to describe multiphase flow modelling, it is required to solve the flow governing equations together with the turbulence model. In this context, the flow governing equations and turbulence model for air-water simulation are presented in this section.

3.1. Governing equations

The VOF method and $k - \omega$ SST turbulence models are applied for modelling stratified gas-liquid flow in the pipeline. The flow is assumed to be incompressible, isothermal and adiabatic. The VOF method, which is a one-fluid approach, comprises the continuity and momentum equations which are given in Equations (1) and (2), respectively (Chinello *et al.*, 2019):

$$\frac{\partial \rho}{\partial t} + \nabla \cdot (\rho \vec{v}) = 0 \quad (1)$$

$$\frac{\partial}{\partial t} (\rho \vec{v}) + \nabla \cdot (\rho \vec{v} \vec{v}) = -\nabla p + \nabla \cdot (\bar{\tau} + \bar{\tau}_t) + \rho \vec{g} + \vec{F} \quad (2)$$

where ρ is the density of the mixing fluids, kg/m^3 ; t is time, s ; \vec{v} is velocity vector after Reynolds averaging, m/s ; p is static pressure, Pa ; \vec{g} is gravity force, m/s^2 ; \vec{F} is a source term

196 accounting for the effect of surface tension. The molecular stress tensor $\bar{\tau}$ is given as (Chinello *et*
197 *al.*, 2019; Li *et al.*, 2019a):

$$\bar{\tau} = \mu \left[(\nabla \vec{v} + \nabla \vec{v}^T) - \frac{2}{3} \nabla \cdot \vec{v} I \right] \quad (3)$$

198 where \vec{v}^T is the transpose of the velocity vector, m/s . The turbulent stress tensor for the
199 Reynolds stress $\bar{\tau}_t$ defined with the Boussinesq eddy viscosity approximation is defined as
200 (Chinello *et al.*, 2019):

$$\bar{\tau}_t = \mu_t \left[(\nabla \vec{v} + \nabla \vec{v}^T) - \frac{2}{3} (\nabla \cdot \vec{v} + \rho k) I \right] \quad (4)$$

201 where I is unit tensor, \vec{v}^T is the transpose of the velocity vector, m/s . The surface tension force,
202 \vec{F} , is modelled using the Continuum Surface Force (CSF) method due to Brackbill (1992).

203 The VOF model concept is applied to treat the two-phase gas-liquid as one single mixture in
204 accordance with the previous studies by Lo and Tomasello (2010) and Chinello *et al.* (2019).

205 The density (ρ) and viscosity (μ) are volume fraction weighted mixture quantities:

$$\rho = \alpha_1 \rho_1 + \alpha_2 \rho_2 \quad (5)$$

$$\mu = \alpha_1 \mu_1 + \alpha_2 \mu_2 \quad (6)$$

206 where α_1 and α_2 are the volume fractions of the primary and secondary phases, respectively.

$$\alpha_1 + \alpha_2 = 1 \quad (7)$$

207 The volumetric transport equation for the secondary phase is determined using the following
208 equation:

$$\frac{\partial \alpha_2}{\partial t} + \vec{v} \cdot \nabla \alpha_2 = 0 \quad (8)$$

209 The pressure gradient is determined as:

$$\nabla p = dp/dx \quad (9)$$

210 where p is the pressure fields along the pipe; x is the position variable going along the length of
211 the pipe.

212 **3.2. Turbulence modelling**

213 Selection of an appropriate turbulence model is highly crucial in two-phase gas-liquid modelling
214 (Ali, 2017). Chinello *et al.* (2019) compared numerical simulations with the physical experiment
215 data conducted by Espedal (1998), which revealed that the $k - \omega$ SST model yields better results
216 than both $k - \omega$ and $k - \varepsilon$ models for the air-water flow simulation if turbulence is properly
217 damped at the gas-liquid interface. Therefore, the $k - \omega$ SST model is employed in this study,
218 and its constitutive equations are defined as follows:

219 The turbulence viscosity is given as (Chinello *et al.*, 2019):

$$\mu_t = \frac{\rho k}{\omega} \frac{1}{\max \left[\frac{1}{\alpha^*}, \frac{SF_1}{a_1 \omega} \right]} \quad (10)$$

220 where k is turbulent kinetic energy, J/kg; ω is specific dissipation rate, S is the strain rate
221 magnitude and is defined as:

$$S = \sqrt{2S_{ij}S_{ij}} \quad (11)$$

$$S_{ij} = \left(\frac{1}{2} \right) \left(\frac{\partial V_i}{\partial x_j} + \frac{\partial V_j}{\partial x_i} \right) \quad (12)$$

222 where S_{ij} is the average strain rate, V_i and V_j are the velocity components in x_i and x_j axis,
 223 respectively. The transport equation for the turbulent kinetic energy; k and the specific
 224 dissipation rate ω is defined as:

$$\frac{D\rho k}{Dt} = \frac{\partial}{\partial x_j} \left[\left(\mu + \frac{\mu_t}{\sigma_k} \right) \frac{\partial k}{\partial x_j} \right] + \min(\mu_t S^2, 10\rho\beta^* k\omega) - \rho\beta^* k\omega \quad (13)$$

$$\begin{aligned} \frac{D\rho\omega}{Dt} = & \frac{\partial}{\partial x_j} \left[\left(\mu + \frac{\mu_t}{\sigma_\omega} \right) \frac{\partial \omega}{\partial x_j} \right] + \frac{\alpha}{V_t} \min(\mu_t S^2, 10\rho\beta^* k\omega) - \rho\beta\omega^2 + 2(1 - F_2)\rho \frac{1}{\sigma_\omega, 2\omega} \frac{\partial k}{\partial x_j} \frac{\partial \omega}{\partial x_j} \\ & + S_\omega \end{aligned} \quad (14)$$

225 and the additional source term, S_ω , is given as:

$$(S_\omega) = A\Delta n\beta\rho \left(\frac{B6\mu}{\beta\rho(\Delta n)^2} \right)^2 \quad (15)$$

226 where Δn is cell height normal to the interface, β is turbulence model constant and B is a
 227 turbulence damping tuning parameter. The term A is the interface area density.

228 The blending functions F_1 and F_2 are defined as follows;

$$F_1 = \tanh \left[\max \left(\frac{2\sqrt{k}}{0.09\omega y}, \frac{500\mu}{\rho y^2 \omega} \right) \right]^2 \quad (16)$$

$$F_2 = \tanh \left\{ \min \left[\max \left(\frac{\sqrt{k}}{0.09\omega y}, \frac{500\mu}{\rho y^2 \omega} \right), \frac{4\rho k}{\sigma_{\omega,2} D_\omega^+ y^2} \right] \right\}^4 \quad (17)$$

229 where y is the distance to the closest wall surface, D_ω^+ is dimensionless specific dissipation rate.

230 The model constants are selected according to the $k - \omega$ SST model of Chinello *et al.* (2019).

231 4. Computational field

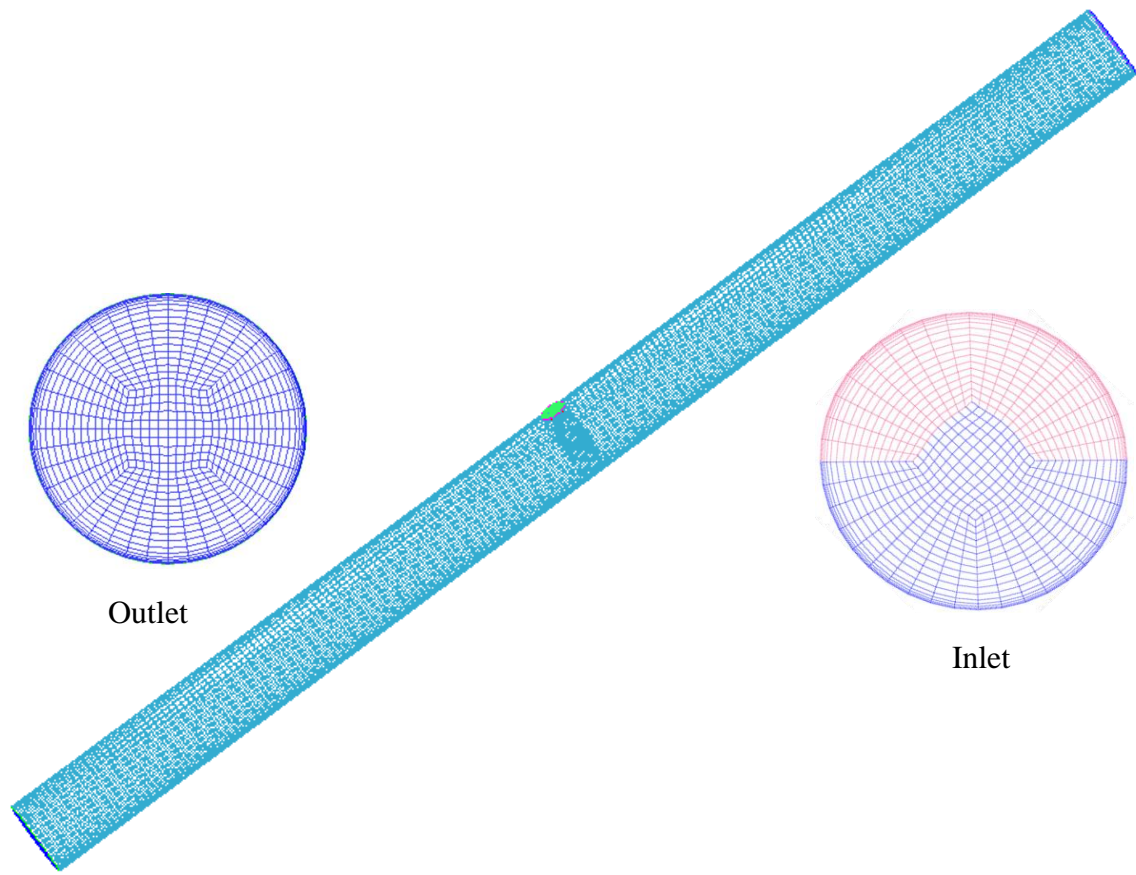
Fig. 1 presents the flow field domain of the proposed pipeline leak assessment modelling. The computational steps include mesh generation, boundary condition definitions, numerical method and code validation. For the results presented in this and subsequent sections, the pipeline inlet is treated as the reference location and all distances are measured relative to the pipeline inlet.

4.1. Mesh generation

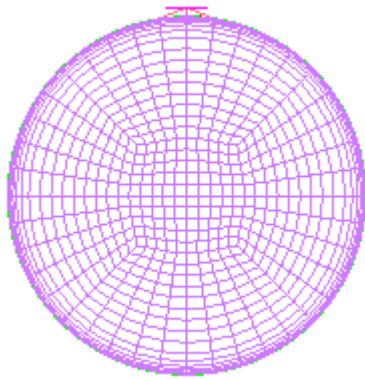
The numerical simulations are conducted on a 3-D horizontal pipeline with and without a leak. A pipe diameter of 0.06 m is employed in this study. The flow domain is divided into small discrete cells and meshed using structured mesh. This grid type allows the mesh refinement to be closer to the pipe wall and provides an opportunity to prevent singularities at the middle of the flow domain (Akhlaghi *et al.*, 2019). The mesh is generated such that the coarse mesh is in the centre, while the fine mesh is at the region near the pipe wall, as recommended by Akhlaghi *et al.* (2019). The mesh was developed using advanced functions, which resulted in its high quality with an average orthogonal quality of 0.99 (closer to 1.0) and skewness of 0.06. A grid dependence test was performed using various grid sizes to identify the most efficient grids for this study. In the grid independence study, superficial gas and liquid velocities were chosen as 3.0 m/s and 0.32 m/s, respectively, which are similar to the numerical simulation values employed in Chinello *et al.* (2019) and physical experiment on stratified flow conducted by Espedal (1998).

The mesh independence analysis was performed by running simulation on grids with the smaller cells number. The grids size was further reduced, which subsequently led to the increases in grids number. Note that a mesh independent solution exists once changing in mesh size does not affect the final simulation. The grids sensitivity was performed by increasing the mesh sizes at

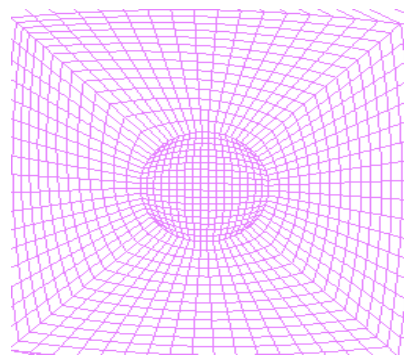
the cross-section of the pipe and along the pipe axis. Table 1 details the specifications of the employed grids, including its cross-sectional number and axial mesh cells. The mesh density effects are studied on the pressure drop characteristics. Fig. 2 (a) illustrates pressure drops at 1.5 m away from the pipe upstream for the 3 m pipe with the 60 mm diameter. The figures show the pressure behaviours of mesh 1 to mesh 4 for the 20 s numerical simulation. The simulation results show that increases in grid numbers from mesh 2 to mesh 4 has little changes on the pressure drop, whereas the difference between mesh 1 and the other mesh sizes is massive. The pressure drop per unit length for the different mesh sizes at locations 1, 2 and 3 is shown in Fig. 2(b). The figure indicates that the pressure drop does not change significantly between meshes 2, 3 and 4. Therefore, mesh 2 was chosen for the numerical simulation as it demonstrates the optimum cells number for this study. Besides the simulation results' accuracy, simulation cost is essential to consider before one chosen mesh sizes for the simulation study. Therefore, mesh 2 demonstrate the optimum mesh size for the present study as it satisfies both computational cost and accuracy.



(a) Mesh generation for modelling pipeline leakage



(b) Cross-section view of the leakage

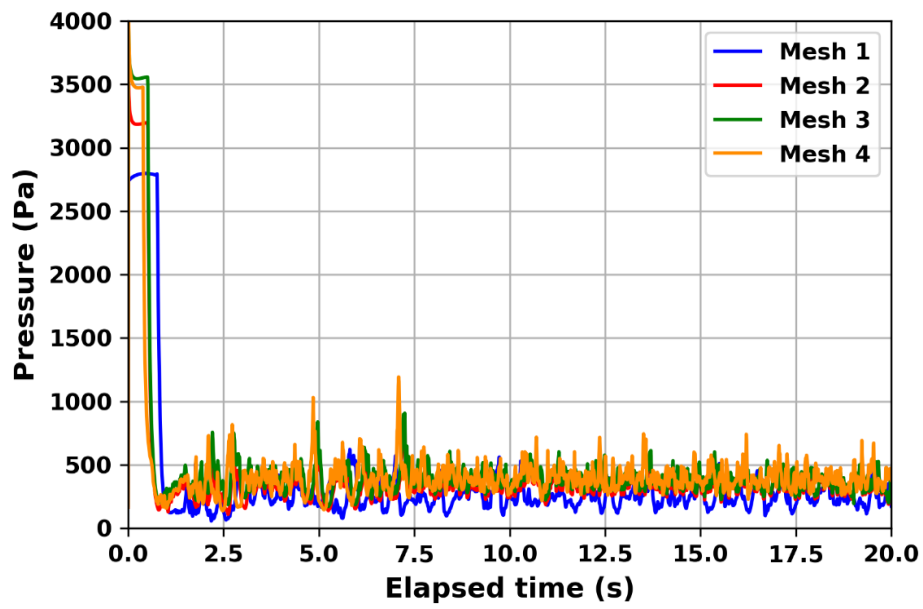


(c) Top view of the leakage

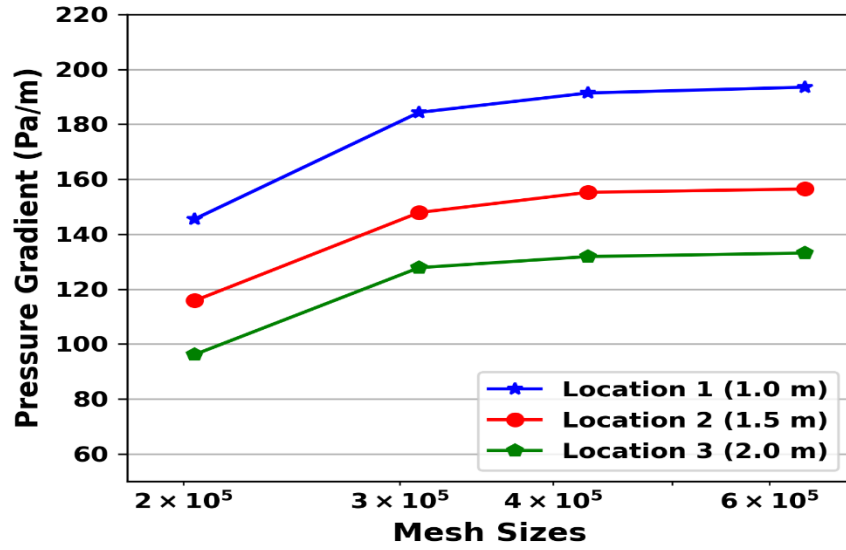
Fig. 1. Depiction of the mesh duct and detail of (a) Mesh generation for modelling pipeline leakage, (b) Cross-section view of the leakage and (c) Top view of the leakage

Table 1: Grids specification for mesh sensitivity analysis

Mesh name	Cross-sectional	Axial cells	Total
Mesh 1	511	400	204,400
Mesh 2	778	400	311, 200
Mesh 3	1067	400	426,800
Mesh 4	1603	400	641,200



(a)



(b)

Fig. 2: Influence of variations in mesh density on model predictions: (a) mesh independency for pressure drop at 1.5 m from the pipeline inlet, and (b) mesh size against pressure gradient across selected locations along the pipe. Note that locations 1, 2 and 3 are set at 1.0 m, 1.5 m and 2.0 m, respectively, away from the pipe upstream.

4.2. Boundary conditions

The pipeline inlet is set as a velocity inlet boundary defined by gas and liquid superficial velocities. Injection of the two-phase into the computational domain can be done in two ways. One method is to set the maximum velocity and non-slip volume fraction as boundary conditions. After some distance, the separation between the mixed phases initiates along the length of the pipe and distributes fluids into a specific pattern. In the second approach, which is the method used in this study, the two phases are separately injected at the pipe inlet. One significant advantage of this method is that flow can reach the fully developed condition sooner. The gas is injected from the upper half cross-section of the pipe, while the liquid is injected from

the bottom half cross-section of the pipe. This resembles a separate flow structure, where each phase is separated into different layers, with the lighter fluid flowing on top of the denser fluid. The gas and liquid velocities at the inlet are specified to attain the target superficial velocities of the phases based on experimental data.

The physical properties of the fluid phases are presented in Table 2. The leak boundary is set as pressure outflow. The no-slip condition is applied at the pipe wall. Since the flow is assumed to be fully developed at the pipeline outlet, the backflow boundary pressure is imposed. The pipe is assumed to be in underwater condition, and the leak orifice and pipeline outlet pressures are defined constant, which is similar to that reported in Kam (2010) for pressure at 100 m below the sea surface (Wei and Masuri, 2019). In this instance, the pipeline outlet and leak surrounding pressures are scaled down to 400 Pa based on pipe diameter and simulation parameters in the present study.

Table 2: Fluid phases of physical properties

Property	Gas-phase	Liquid-phase
Density (ρ), kg/m^3	1.225	998.2
Dynamic viscosity (μ), Pa.s	0.00001823	0.00091
Interfacial tension, N/m	0.0715	

4.3. Numerical method

The VOF modelling method is employed to simulate stratified gas-liquid flows. The computation is performed using a pressure-based solver, while the pressure fields are coupled with the velocity fields using SIMPLE pressure-velocity coupling scheme. The turbulence is modelled

using the $k - \omega$ SST model. The time-step used in the simulations is 0.001 s, and the simulated for 20, which is 20,000 iterations. All the computation run on an Intel(R) Xeon(R) Gold 6230 CPU @ 2.10GHz, 16 Cores, 64.0 GB RAM. Please note that a single simulation required five days on average to complete on this computer. The momentum, turbulent kinetic energy and specific dissipation rate equations are discretised in space for the advection terms using a second-order upwind scheme in accordance with the study of Chinello *et al.* (2019). The discretisation of the volume fraction is performed using high-resolution interface capturing (HRIC) scheme (ANSYS, 2017). A first-order implicit temporal discretisation scheme is used to solve the governing equations. This method has been demonstrated to be reliable for evaluating pressure gradients and flow rates which are of interest in this work (Chinello *et al.*, 2019). The implicit algorithm is applied because the time derivative estimation can be obtained from neighbouring cells, which allows numerical calculation stable unconditionally with respect to the time-step size (Ali, 2017).

4.4 Comparison with experimental data from the literature

4.4.1 Code validation

The CFD code used in this study has been validated against the published experimental data in Espedal (1998) and numerical simulations reported in Chinello *et al.* (2019), which also employed the VOF model in ANSYS. Simulations are conducted using the VOF model for stratified air-water flow in a 3D pipe with the same experimental conditions as in these studies. The pipe used for the simulations is 18 m in length with a diameter of 0.06 m. The values of the model parameters for the density, interfacial tension and dynamic viscosity are given in Table 2. The $k - \omega$ SST turbulence model with the damping factor (B) of 250 is employed. Four sets of

numerical simulations were performed using the superficial gas velocity of 3 m/s, while the superficial liquid velocities were chosen as 0.12 m/s, 0.18 m/s, 0.26 m/s and 0.32 m/s. The pressure gradients are computed and compared against the experimental data. Fig. 3(a) shows the comparison of the present simulation results against the numerical simulations reported in Chinello *et al.* (2019), and experimental data reported in Espedal (1998). The obtained results demonstrate good agreement with the published CFD simulation results and experimental data. As shown in Fig. 3(a), the pressure gradient in the present simulation is more consistent with the experimental data than the simulation results reported in Chinello *et al.* The reason for the underestimation of liquid levels in Fig. 3(b) could be inherent from the liquid injection surface area of the pipe (see Fig. 1 for the inlet cross-section plane in boundary condition). Therefore, it should be admitted that there is a discrepancy in liquid levels obtained in both simulation and experiments due to the possible difference in the surface area of injection of the liquid phase. This validation has been undertaken to demonstrate the adequacy of the mesh and numerical schemes employed. In order to further ascertain the validity of our model, the predictive accuracy of the present simulations was tested against the experimental data of Strand (1993). Fig. 4 show comparisons of the pressure gradient between the current simulation and corresponding experiments data of Strand (1993). As shown in Fig. 4, the prediction matches the measurement data very well, with a deviation of less than 5%.

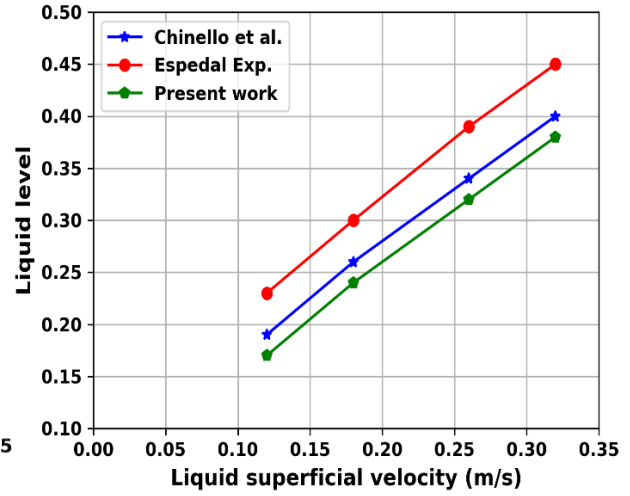
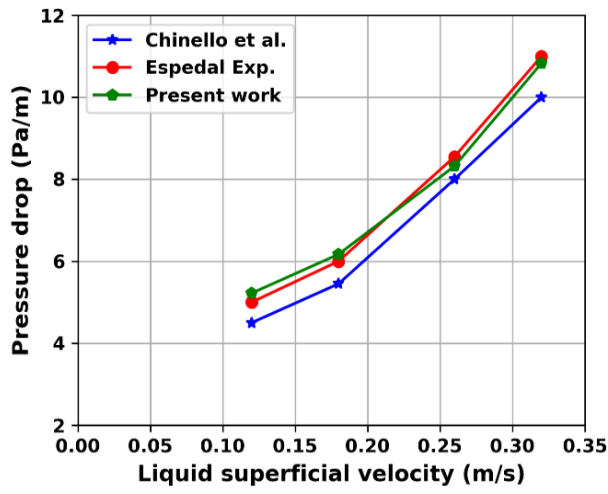


Fig. 3. Validation of numerical simulation model against experimental data reported in Espedal *et al.* (1998) and numerical simulation results in Chinello *et al.* (2019); (a) pressure drop (Pa/m), (b) Liquid level.

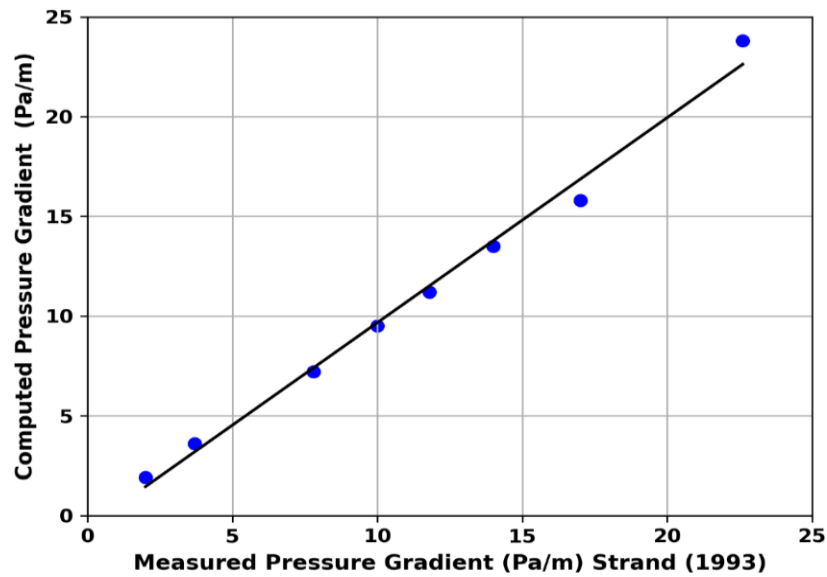


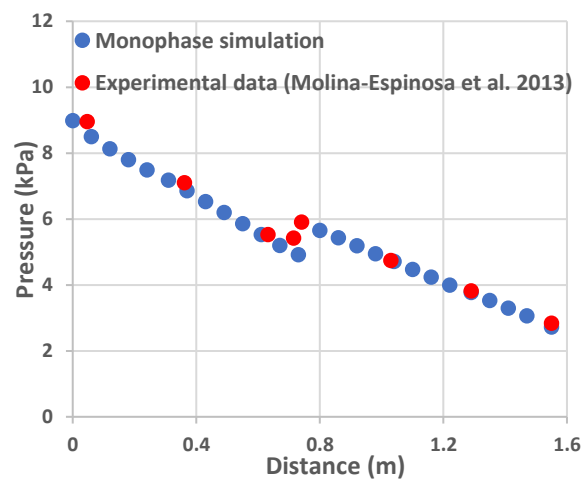
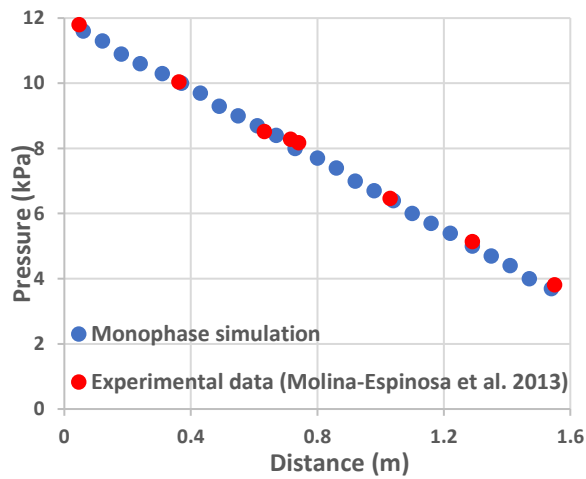
Fig. 4. Comparison of pressure gradient between current simulation and corresponding experiments data of Strand (1993)

4.4.2 Pipeline leaks comparison against experimental data

Experimental data focused on the multiphase pipeline with the leak is seldomly reported and it is not easy to set up flow ring similar to the one reported in Molina-Espinosa et al. (2013), to test the gas-liquid, such as hydrocarbon and oil physical facility. The experimental data obtained from the same geometric model and simulation conditions in monophasic systems employed to verify that the boundary conditions. The pressure distribution proved effective and scientific to characterise stratified flow behaviours in this study. The effect of leak on stratified flow behaviours induced by leaks has previously observed similar to the monophasic pipeline leakage in the previous study (Figueiredo et al. 2017). They concluded that the leak localisation strategy based on the upstream and downstream pressure profiles commonly employed in monophasic flow pipeline leakage could be extended to the stratified-flow system. However, all the data reported in that study was based on the 1-D pipeline.

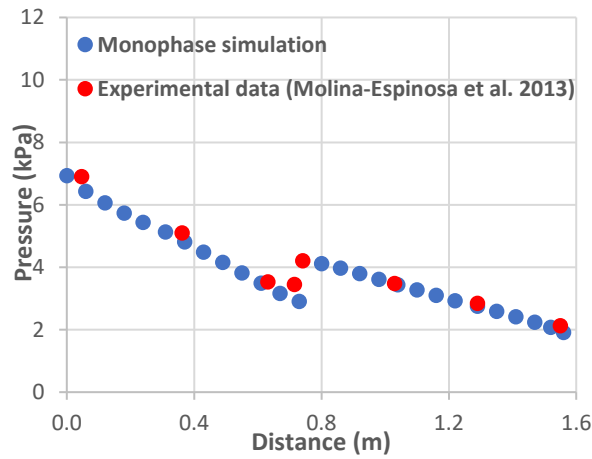
The present stratified flow model carried out in a 3-D pipeline is compared with the monophasic flow system and validated with the experimental data reported by Molina-Espinosa *et al.* (2013). Molina-Espinosa *et al.* (2013) measured pressure distribution for the leak-free and leak diameters of 0.0033, 0.0052 and 0.0074 m, which form the leak sizes considered for the validation in the present study. The pipeline could be hundreds or thousands of meters long in reality; however, irrespective of the length of the pipeline, the pressure gradient would remain the same under normal flow condition. Therefore, a comparison between the simulation results obtained from the pipeline length considered in the present study and experimental data presented in (Molina-Espinosa et al. 2013) is scientifically sound.

The comparison of the pressure profile between experimental data and monophasic results is shown in Fig. 5. The pressure profile without leak is illustrated in Fig. 5(a), and the resulting pressure profile with leak sizes 0.0033, 0.0052 and 0.0074 m are shown in Fig. 5(b), Fig. 5(c), and Fig. 5(d), respectively. Fig. 6 compares stratified flow against monophasic results in Fig. 5. The monophasic and stratified flow models are set up based on the experimental configuration for validation (Molina-Espinosa et al., 2013). As shown in Fig. 5, the monophasic simulation results agree with the experimental data conducted on a single-phase scenario at a higher degree. The pressure profile correlation in Fig. 6 reveals a slight divergence. The reason is that the stratified model is made up of gas-liquid phases, leading to the gas release rate probably higher than the liquid quantities under the same leak size. Statistical tests are applied to verify the consistency among pressure data obtained from the monophasic simulation, stratified flow simulation and experiments reported in Molina-Espinosa et al. (2013).

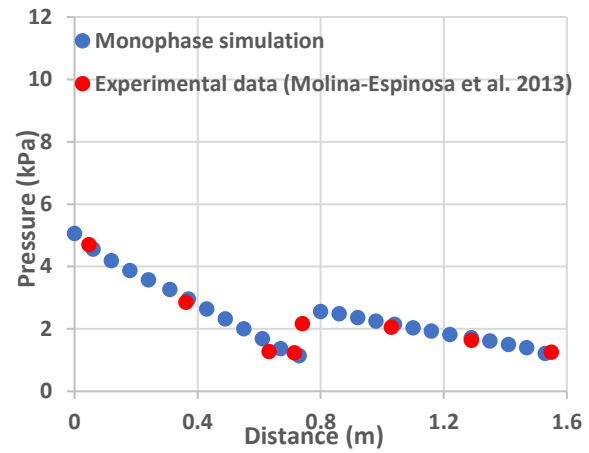


(a)

(b)

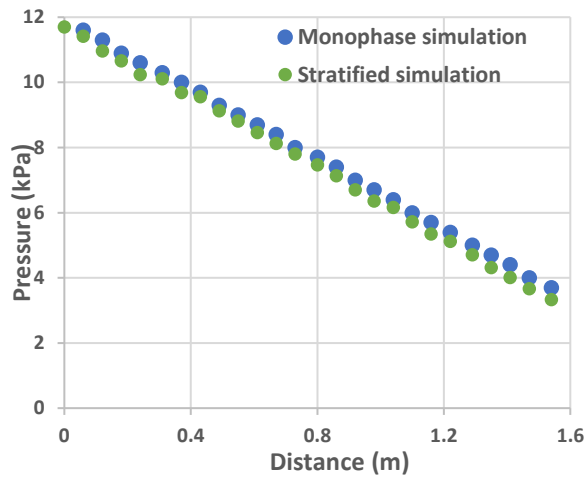


(c)

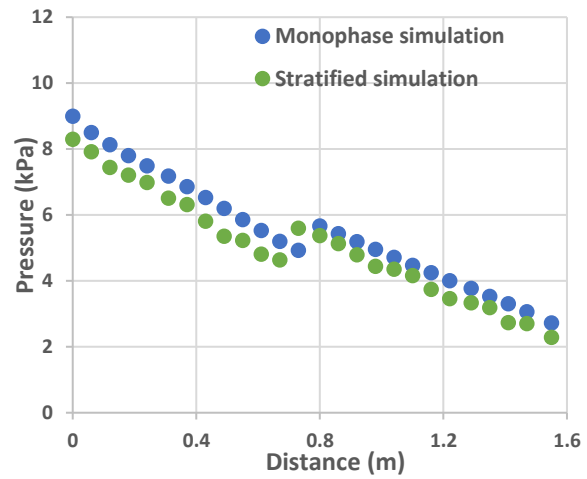


(d)

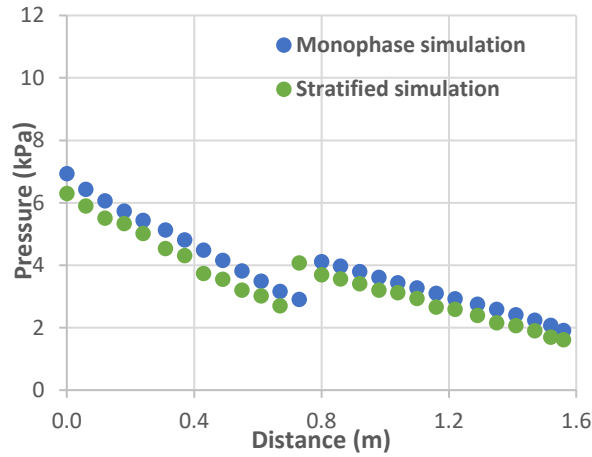
Fig. 5: Comparison for the pressure profile between the monophasic flow and the stratified flow model; (a) leak free, (b) 0.0033 m leak, (c) 0.0052 m leak, (d) 0.0074 m leak.



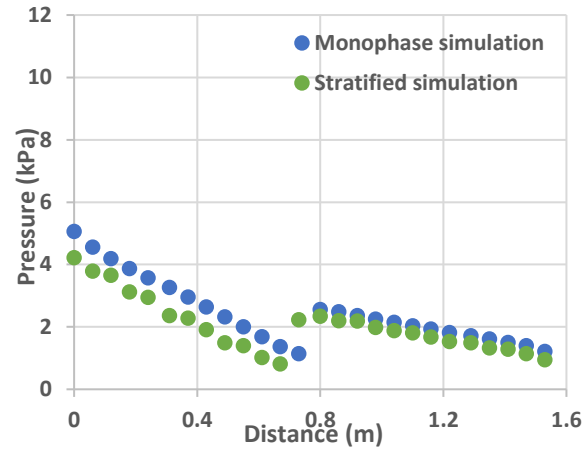
(a)



(b)



(c)



(d)

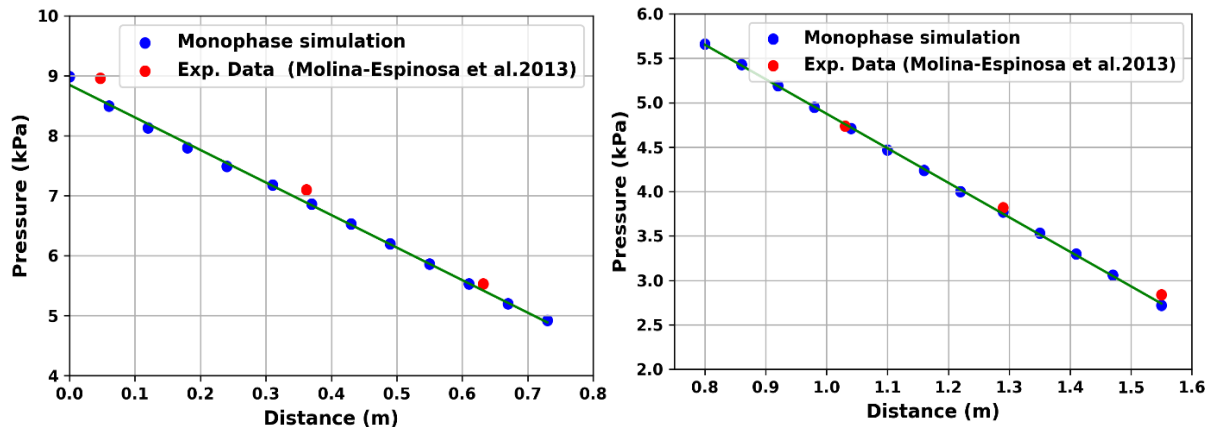
Fig. 6: Comparison for the pressure profile between the monophasic flow and the stratified flow model; (a) leak free, (b) 0.0033 m leak, (c) 0.0052 m leak, (d) 0.0074 m leak.

The statistical analysis was computed in MATLAB 2018b using one-way Analysis of Variance (ANOVA) to compare the pressure gradient before and after the leak. The summary of the hypothesis test results for the monophasic simulations, experimental data and stratified model is presented in Table 3. The p-values measure how much the means different of the three data disagrees with the null hypothesis (the sample means of data taken from the 3 groups are equal). As is clearly shown, the p-values for all the cases are range from 0.131 to 0.734, using 0.05 significance (α) level. These indicate that the mean difference between the three data are not statistically significant and demonstrate strong evidence for the null hypothesis. We fail to reject the null hypothesis at the significant level of 0.05.

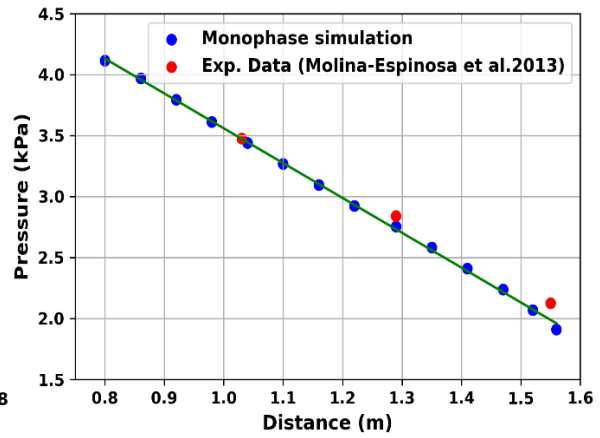
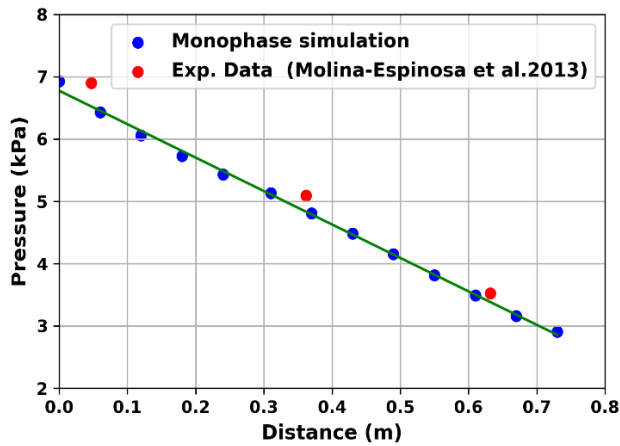
Table 3: Numerical (monophase and stratified) simulations and experimental data comparison using one-way ANOVA; 0.05 significance (α) level

Leak scenario	Pressure gradient	p-values
Leak free	Upstream pressure	0.734
	Downstream pressure	0.747
Leak 1	Upstream pressure	0.382
	Downstream pressure	0.365
Leak 2	Upstream pressure	0.473
	Downstream pressure	0.354
Leak 3	Upstream pressure	0.365
	Downstream pressure	0.131

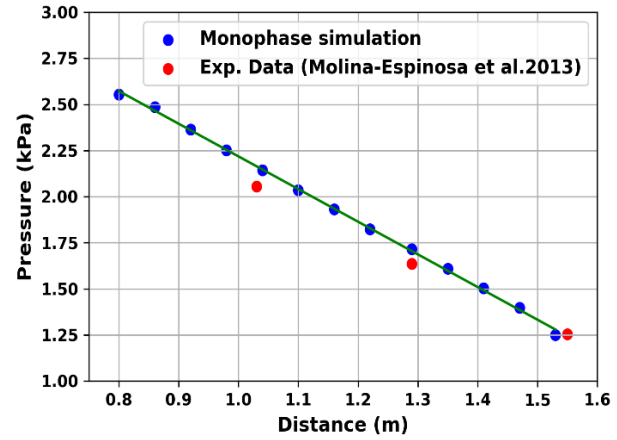
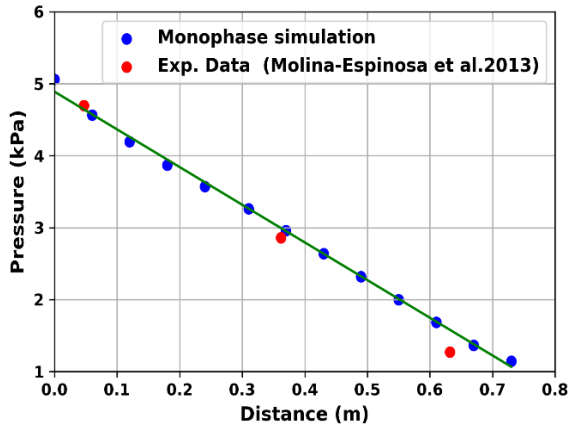
The linear regression plot shown in Fig. 7 demonstrates the adequate closeness of the experimental and monophase simulation data points to the regression model. The average variance of the experimental data from the fitness model is calculated using Mean Absolute Deviation (MAD). The obtained results are presented in Table 4. From these results, the highest MAD value is 0.263, which shows good agreement between the two data.



(a)leak 1



(b) Leak 2



(c) Leak 3

Fig. 7: Linear regression plot for monophase simulation against experimental data. Pressure gradient before leak (left) and pressure gradient after leak (right)

Table 4: The results of computed Mean Absolute Deviation (MAD) of experimental data from monophase simulation regression model.

Leak scenario	Pressure gradient	MAD
Leak free	Upstream pressure	0.060
	Downstream pressure	0.123
Leak 1	Upstream pressure	0.234
	Downstream pressure	0.060

Leak 2	Upstream pressure	0.263
	Downstream pressure	0.089
Leak 3	Upstream pressure	0.149
	Downstream pressure	0.061

Table 5 also presents the results of the hypothesis tests performed to determine whether the constants and coefficients of linear regression models of the monophasic and stratified pressure gradients variation before and after the leak are statistically significant. As demonstrated in the results shown in Table 5, the high R-square values indicate that the fitted linear regression models approximate the process which generates the data well. It is important to notice that the least R-squared value is 0.997 despite the multiphase coefficients p-value higher than 0.05. This indicates the possible disband among the stratified data due to the transient state of the multiphase model. These results agree to the previous study (Figueiredo et al. 2017) that concluded a leak localisation strategy based on the upstream and downstream pressure profiles commonly employed in monophasic flow pipeline leakage could be extended to the stratified-flow model. Therefore, the numerical models and simulation method used in this study have good quality and can well describe the fluids flow parameters distribution of pipeline leakage. Similarly, since multiphase flow system span beyond stratified flow pattern in order to have a better understanding of leak effect in all the multiphase system, comparison of other multiphase flow regimes such as bubble, slug, annular, etc. should be considered in future.

Table 5: Regression hypothesis results for monophasic and stratified simulations comparison

Leak scenario		R-Square	RSME	Constant p-value	Mono. Coef. p-value	Multiphase Coef. p-value
Leak free	Upstream pressure	0.998	0.033	1.0295×10^{-13}	0.043353	0.28861
	Downstream pressure	1.000	0.005	1.7711×10^{-20}	0.0005064	0.054394
Leak 1	Upstream pressure	0.998	0.011	1.902×10^{-12}	0.0020	0.2820
	Downstream pressure	1.000	0.004	4.4253×10^{-20}	3.7577×10^{-09}	0.57519
Leak 2	Upstream pressure	0.998	0.009	4.774×10^{-13}	0.0020	0.0690
	Downstream pressure	0.998	0.014	7.8827×10^{-19}	1.2721×10^{-06}	0.75957
Leak 3	Upstream pressure	0.998	0.012	1.305×10^{-11}	0.0010	0.1890
	Downstream pressure	0.997	0.021	3.1492×10^{-14}	0.0008683	0.84597

5. Results and Discussions

Numerical simulations are performed on a 3-D horizontal pipe with different leak scenarios. Holes on pipe which are sources of leaks are assumed to be circular, and its distribution sizes are determined based on International Association of Oil and Gas Producers (IOGP) recommended hole sizes for subsea pipelines (Li *et al.*, 2018). According to the pipeline opening sizes description specified in Li *et al.*, for a standard subsea pipeline with an average diameter of 0.334 m, a leak diameter of less than 0.02 m is regarded as a low leak. Moreover, a leak size between 0.02 to 0.08 m is classified as medium leakage, while a leak diameter higher than 0.08 m is regarded as a large leak. The computed pipe opening dimensions for the 0.06 m diameter pipe employed in this study follow the recommended values in IOGP and they are listed in Table 6. The superficial gas and liquid velocities used for pipeline leak modelling are 4.5 m/s and 0.5

m/s, respectively, while the pipeline length is 50 times the diameter. These values are determined using the horizontal gas-liquid flow regime map so that stratified flow pattern is observed (Kanin et al., 2019). The effect of leak sizes, longitudinal leak locations, axial leak positions and multiple leakages are investigated, and results are presented for the flow rate, pressure gradient and volume fractions in this section.

Table 6: Hole diameter used for the simulations

Hole size classes	Values (mm)	Leak size (percentage of pipe diameter)
Low	1.5	2.5%
Medium	9	15%
Large	14.5	24.2%
Rupture	18	30%

5.1. Effect of leak magnitudes

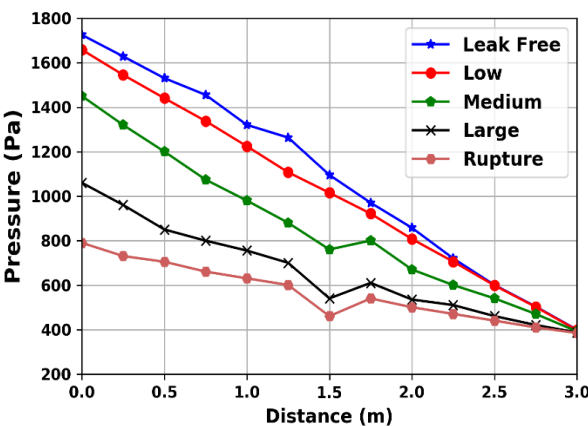
Leak size has a significant impact on the behaviour of fluids flow in the pipeline. In order to study the effect of leak magnitude on the multiphase flow behaviour induced by the leak, simulations of pipeline leakages for the different leak scenarios corresponding to the low, medium, large and rupture scenarios are conducted and analysed. The leak is placed at the top-middle part of the pipe, as shown in Fig. 1. Table 6 presents the values of the leak sizes considered and its corresponding categories. The effects of leak size on the pressure gradient, the flow rate and the volume fraction (gas void fraction and liquid holdup) at selected planes along

the pipeline are presented. The pressure response to the pipeline leak and how the response changes with leak sizes is shown in Fig. 8(a). As seen in Fig. 8(a), the pressure gradient remains identical under the leak-free scenario. The occurrence of leak leads to the reduction in pressure fields as the fluids try to escape through the leak. Although the existence of small leak leads to the decrease in pressure at the upstream of the pipe, the effect of the small leak is not significant at the leak location. This agrees with the analytical calculation in Kam (2010), which affirmed that the presence of a small leak is not visible at the location of the leakage. However, as the pipe leak opening size increases, more fluids tend to discharge through the orifice region. The similar pressure response can also be observed in physical experiment data reported in Molina-Espinosa *et al.* (2013) conducted on single-phase leakages.

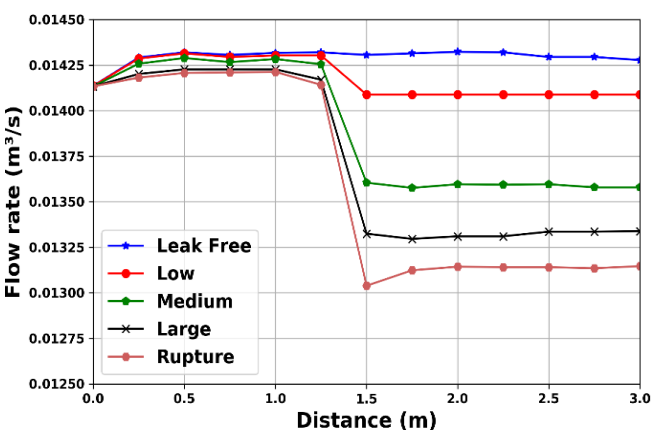
As exemplified in Fig. 8(a), the magnitude of the pipeline opening size affects the rate of fluids discharge in the leak neighbourhood. The increase in fluids escaping from the leak medium leads to the rise in pressure drop, particularly within the vicinity of the leakage. This implies that the pressure profile around the neighbourhood of the leak can aid the accurate identification of leak location particularly when the leak is medium size or large. The presence of large leak size reveals that the larger the size of the leak, the more the fluids tend to discharge from the pipeline until it reaches the rupture stage. The effect of leak sizes on total flow rate characteristics based on various leak diameters is depicted in Fig. 8(b). It can be observed that the maximum decrease in flow rate suddenly occurs immediately after the leak position. There is no much significant variation in flow rate before the occurrence of leakage, but as the size of the leak increases, the fluids flow rate also reduces dramatically starting from the leak location. Therefore, the increases in pipe opening size result in the decrement of total flow rate downstream of the leak. This implies that flow rate decreases with increasing leak size. From the flow responses depicted in

Fig. 8, we conclude that upstream pressure serves as a pertinent indicator to detection of leakage as it appears to be the most sensitive indicator even if the size of the leak is small. Whereas, downstream flow rate response will be more favourable for leak detection if the flow transducer is deployed downstream.

Fig. 9 presents the volume fraction contours at 2.5 m along the pipe under the same leak scenarios shown in Fig. 8. The blue colour denotes the air void fraction, while the red indicates the liquid holdup. As seen in Fig. 9(a), the air void fraction and the liquid holdup are distributed equally in the absence of leakage. The occurrence of leak leads to the reduction in air void fraction downstream of the pipe, which causes an increase in the liquid holdup. By comparing the fluids volume fraction under different leak sizes shown in Fig. 8, it shows that leak size has a significant influence on the saturation of fluids flow. Overall, the larger the leak size, the more the relative amount of gas discharged from the pipeline if the leak is located at the top upper part of the pipe. Therefore, the gas void fraction downstream of the leak becomes lower, which eventually increases the liquid holdup. This occurs because the gas is less dense and more mobile than liquid leading to the liquid replacing the escaped gas in the pipeline.



(a)



(b)

Fig. 8. Leak sizes variation simulations response; (a) pressure distributions, (b) flow rate. Note that the flow rate represents the total flow rate for the two-phases. Note that leak is located at $x/2$, where x is the pipe length.

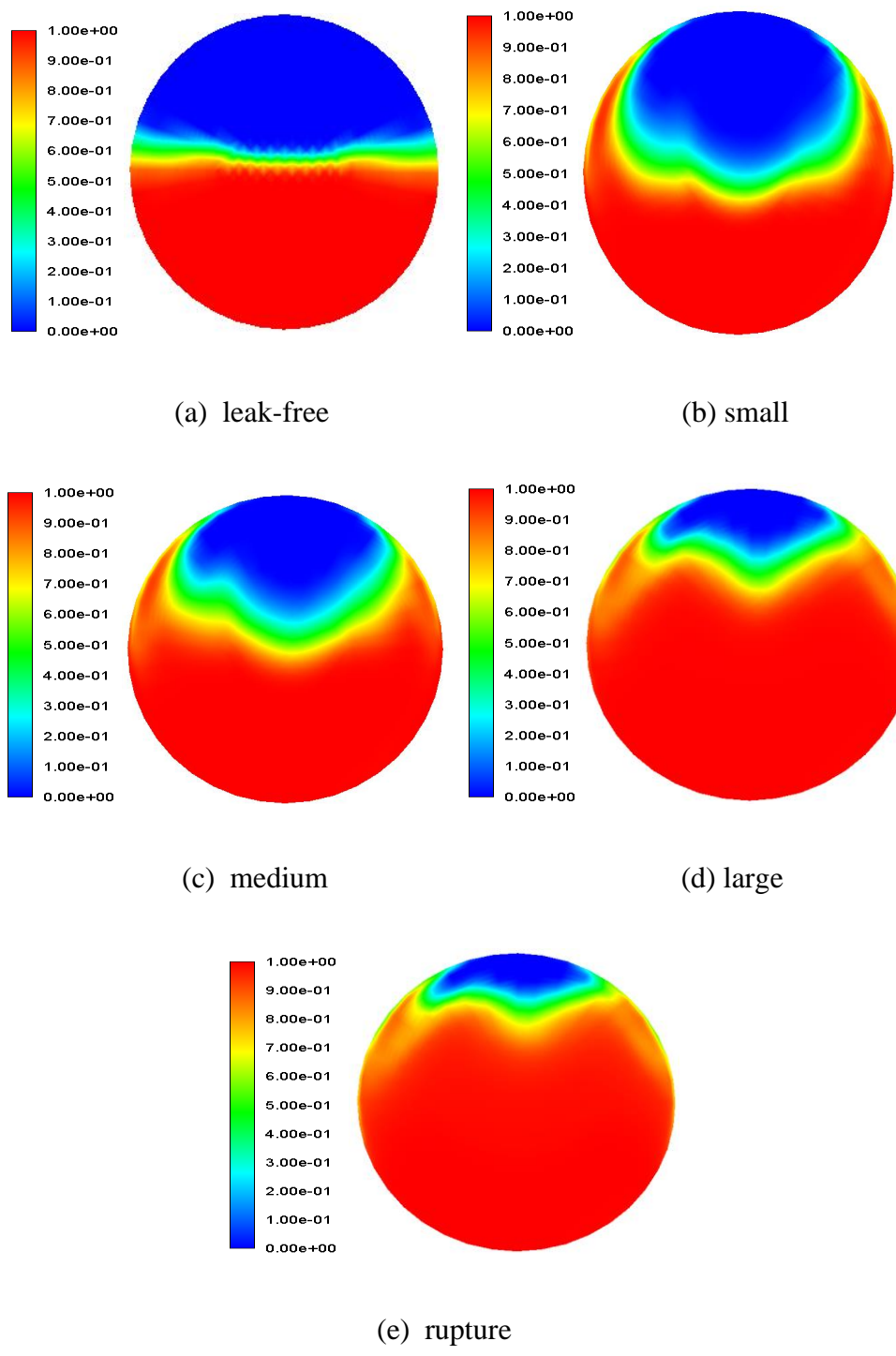


Fig. 9. Liquid volume fraction contour plots at 2.5 m for different leak opening sizes (Red and blue colours indicate water and air, respectively)

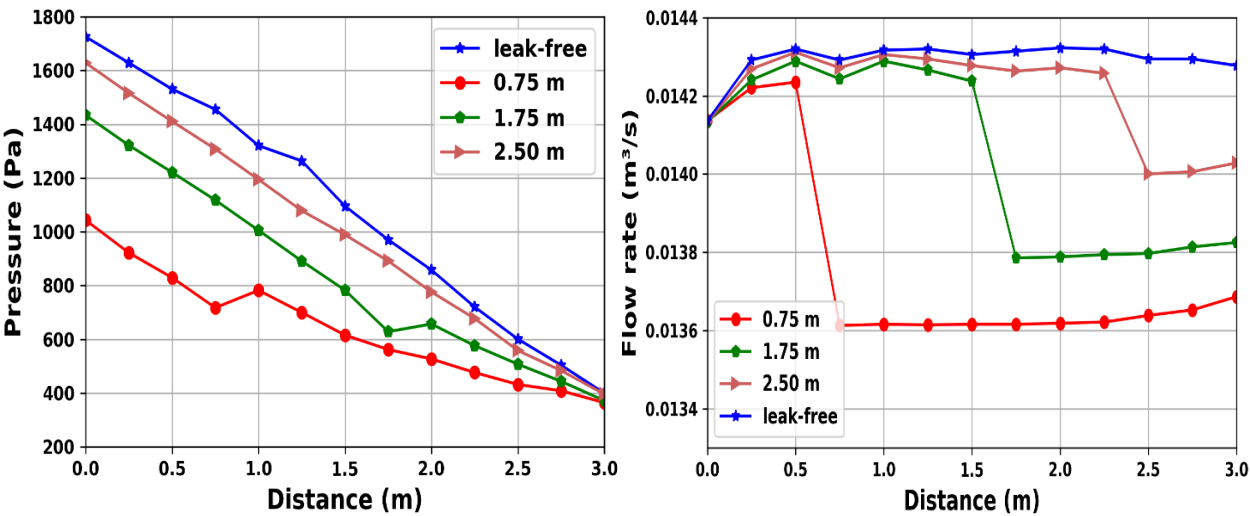
5.2 Effect of longitudinal leak location

Various challenges may be experienced in the process of identifying the position of leakage along a pipe, especially if the pipeline is installed underground or in a subsea environment. Therefore, it is important to investigate the effect of leak on different locations along the pipe length for enhancing leak assessment and emergency planning. In this study, the effect of leak on different longitudinal locations is investigated and analysed. The leak location 1, location 2 and location 3 are set at 0.75 m, 1.75 m and 2.5 m, respectively away from the pipe upstream. Fig. 10 presents the effect of longitudinal leak detection on the medium pipeline opening size for the pressure and flow rate responses. Fig. 10(a) shows the effect of different longitudinal leak locations on the pressure profile. As seen in Fig. 10(a), the occurrence of leakage toward the downstream of the pipe (at 2.5 m) has little effect on the pressure gradient. However, as the leak is positioned more towards the upstream section of the pipe, the leak effect become pronounced. Similar responses have also been observed in the analytical solution in multiphase pipeline leakage reported by Kam (2010).

As it can be observed in Fig. 10(b), the occurrence of leak leads to the flow rate decrement starting from the leak position downward to pipeline outlet. The leak occurred at 2.50 m away from the upstream pipeline cause about $0.00024 \text{ m}^3/\text{s}$ flow rate reduction. By positioning a leak further upstream of the pipeline, the effect of a leak becomes more pronounced. This agrees with the analytical solution reported in Kam (2010). If a leak occurs closer to the pipeline upstream, it is more favourable to detect the leak using the inlet pressure monitoring. The result of the liquid

holdup is illustrated in Fig. 10(c). As it is clearly shown, the loss of pressure as the leak location closer to the upstream of the pipe reveals increases in liquid holdup accordingly. Fig. 10(d) shows a comparison of published liquid holdup (Figueiredo *et al.* 2017) against the result in Fig. 10(c). the figure reveals a correlation in relative jump, particularly as the leak closer to the pipeline downstream.

The volume fraction contour plots at 2.75 m for the longitudinal locations are illustrated in Fig. 11. By comparison, a significant difference can be found in volume fraction as the location of leakage changes from the pipe upstream to the outlet. In the absence of leakage, the fraction of each phase distributes equally. However, the variation in leak position results in liquid accumulation increasing as the leak location changes toward the upstream of the pipeline.



(a)

(b)

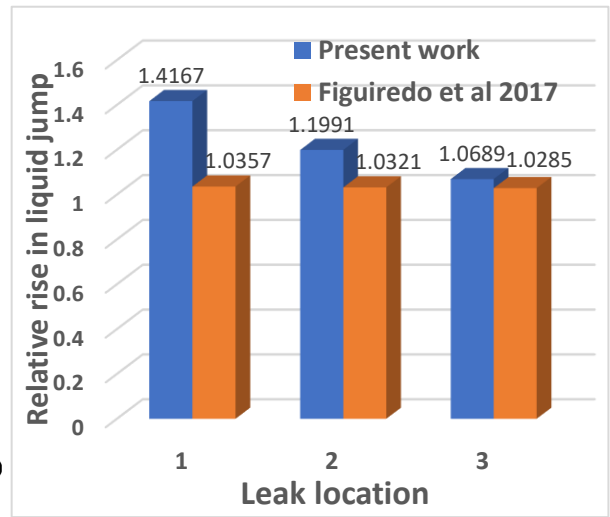
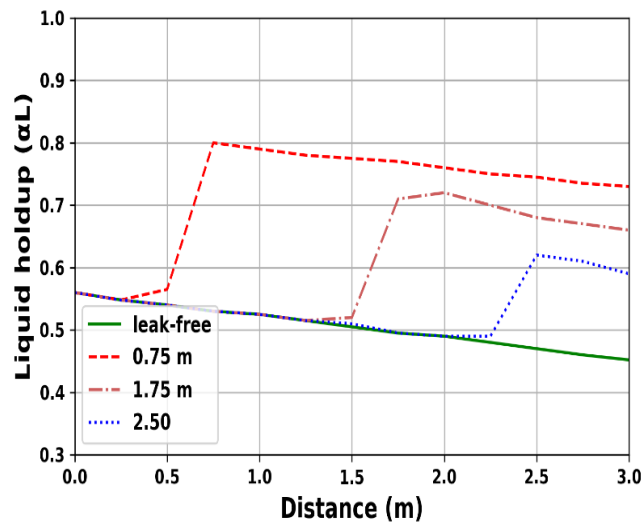
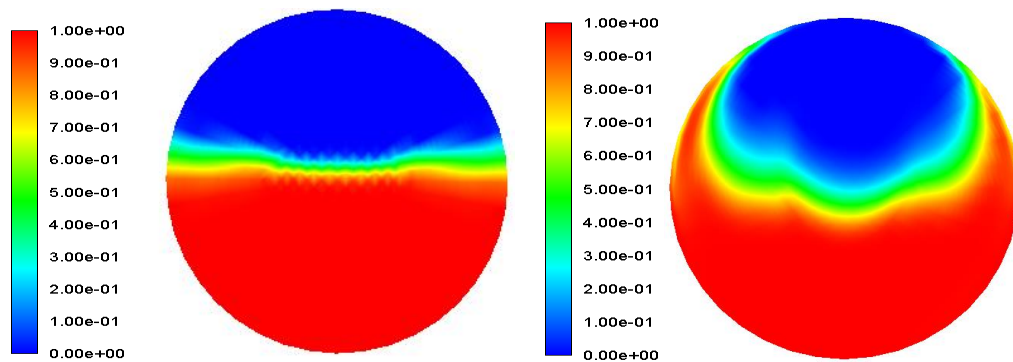


Fig. 10. Effect of longitudinal leak locations; (a) pressure distributions, (b) flow rate, (c) liquid holdup, (d) liquid holdup comparison with published data. The legend shows different locations of leakage from pipe upstream to the downstream. Note that the flow rate represents the total flow rate for the two-phases.



(a) leak-free

(b) 2.50 m

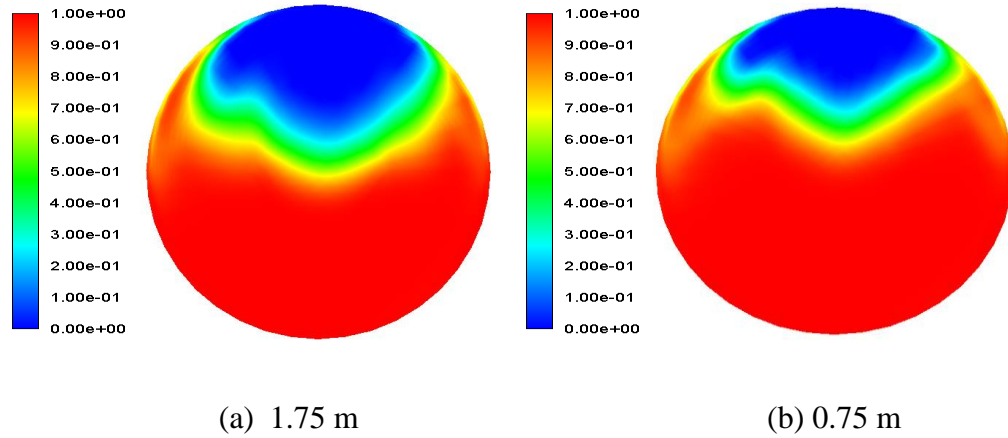


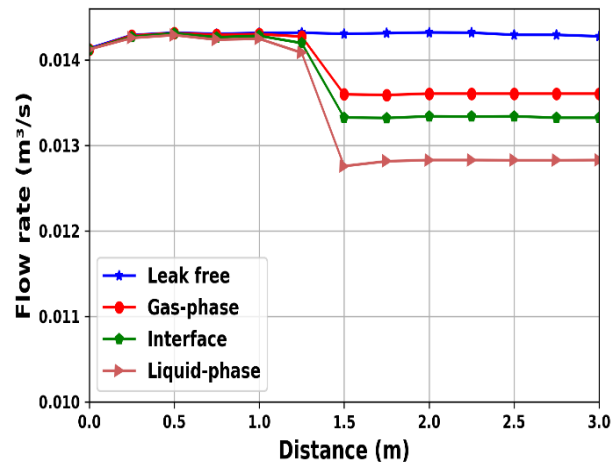
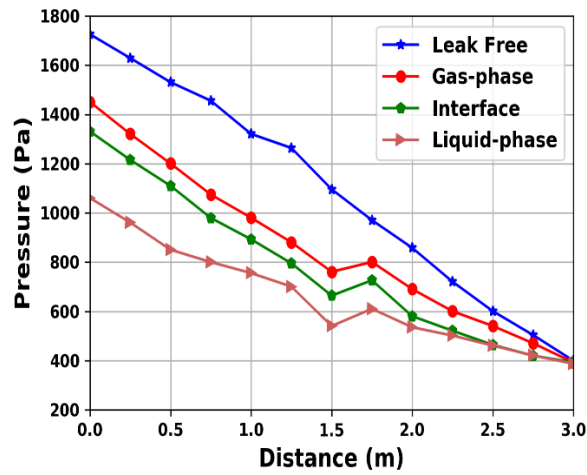
Fig. 11. Volume fraction contour plots at 2.75 m for different longitudinal leak locations. (Red and blue colours indicate water and air, respectively).

5.3 Effect of axial leak positions

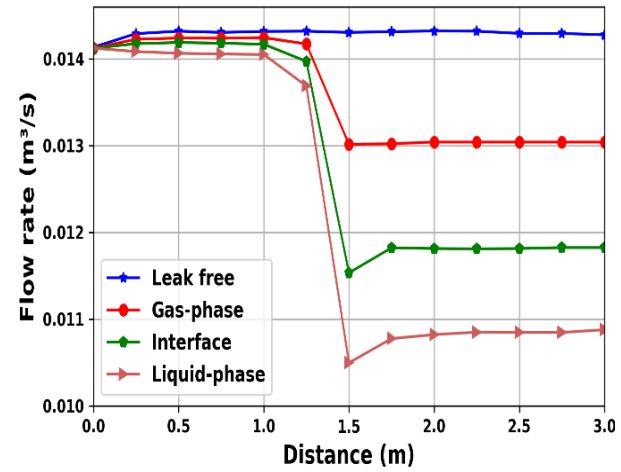
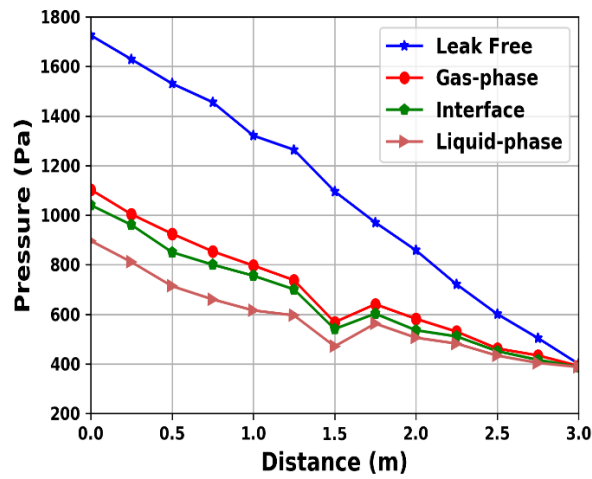
In the previous section, the leak was set to locate in the gas phase. Knowledge about pipeline leak position, namely gas-phase, liquid-phase or interface of the two phases is important for enhancing the understanding of leak effect on a multiphase pipeline system. The leak scenarios for the medium and large sizes are considered to study hydraulic behaviours induced by leak at different fluid phases. The leak is located at the middle of the pipe, as shown in Fig. 1. The legend indicates the fluid phases where the leak occurred. The flow parameters that are investigated include the pressure gradient, the total flow rate and the volume fraction of the fluids within the pipeline. The flow parameters variation for the medium leak size under different leak positions is presented in Fig. 12(a). The legend indicates the fluid phases where the leak occurred. As seen in these figures, it is apparent that the location of leakage on the multiphase pipeline affects the flow pressure profile in the pipeline. A significant effect exists when the leak

is situated on the liquid-phase side. Similarly, the flow rate responses in Fig. 1(a) imply that the maximum total flow rate drop occurs at the liquid-phase axis, while the least drop is observed at the gas-phase position. Similar behaviour for the case of large leak can also be observed in Fig. 12(b).

By comparison, we can find that the influence of pipeline leakage is more pronounced on the liquid phase than gas or gas-liquid interface, and the reasons are two-fold. Firstly, the leak at the bottom of the pipeline (liquid-phase) favours the quantity of the pipeline's fluid discharge. Secondly, the fluids' physical properties could also be another reason for the higher pressure drop in the liquid phase. For instance, the high density of the liquid may be one of the factors contributing to the higher pressure drop when the leak is situated in the liquid phase. The gas-liquid volume fraction distribution for the leak at the gas-phase, liquid-phase and interface of the two phases are examined using contour plots at 2.5 m away from the pipe upstream. Fig.13 shows the responses of fluids fraction for the same leak scenarios as in Fig. 12(b). The absence of leak shows that the void fraction and liquid holdup is nearly uniform with the clear interface between the liquid and gas phase as previously observed in Fig. 12(a) and (b) for the pressure profile and flow rate responses, respectively. However, Fig. 13(b) shows that the occurrence of a leak at the gas phase attracts liquid moving from the bottom of the pipeline toward the leak region. Fig. 13(c) and (d) present the fluids saturation for the leak event at the gas-liquid interface and liquid phase. The occurrence of a leak at the gas-liquid interface allows air to diffuse into the water as both phases discharge simultaneously from the pipeline.



(a)



(b)

Fig. 12. Effect of axial leak positions; (a) medium size, (b) large size. (Pressure distributions (left) and flow rate (right)). Note that the flow rate represents the total flow rate for the two-phases.

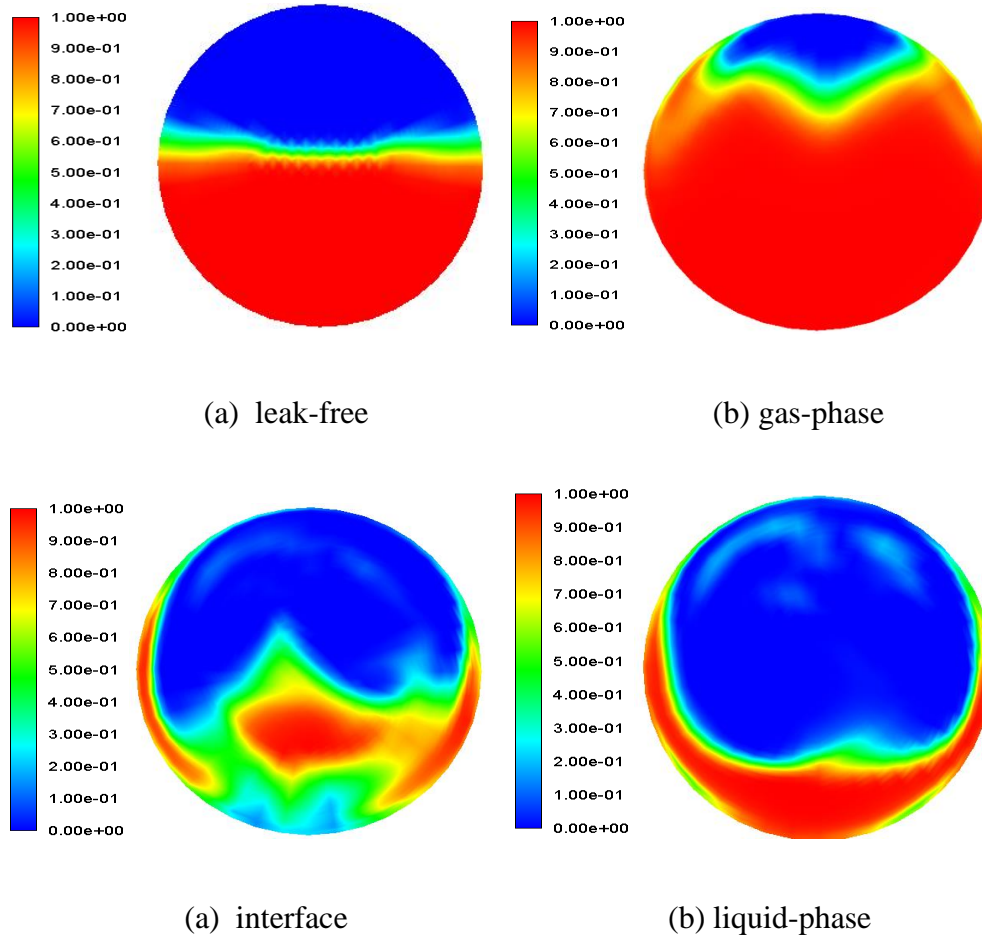


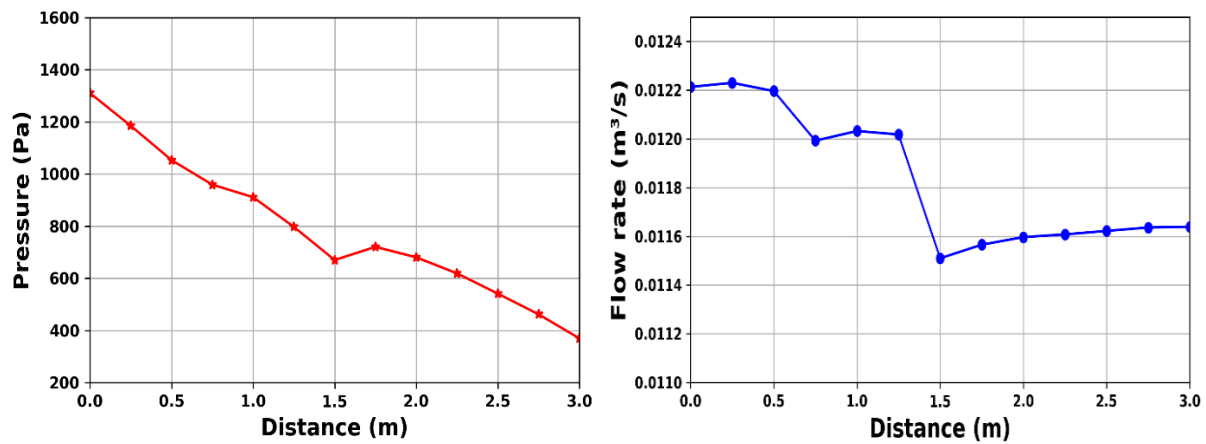
Fig. 13. Volume fraction contour plots at 2.5 m for leak at different axial positions. (Red and blue colours indicate water and air, respectively. The leak is located at the middle of the pipeline).

5.4 Effect of multiple leakages

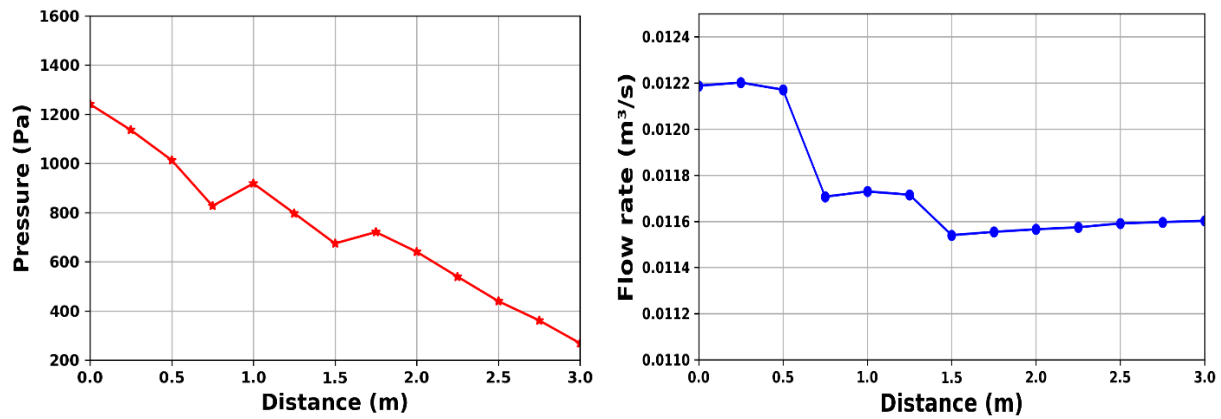
The emergence of double leaks on a single pipeline can easily affect the accuracy of detecting pipeline leakage. Therefore, the investigation of multiphase flow in pipe with multiple leaks plays a crucial role in determining the size of the leaks and identify the location of pipeline leakage accurately. The impact of double leaks on pipeline leak detection and localisation has been considered and analysed in this study. Fig. 14 illustrate the pressure gradients and the flow

rates in various multiple leak scenarios. The first leak location is set at 0.75 m away from the pipe upstream, while the second leak is located at the 1.5 m, which is the mid-point of the pipeline. The two leak sizes are chosen among small, medium and large. In all scenarios, the second hole is chosen to have a medium size. Fig. 14(a), shows the double leak scenario where the first leak has a small size. The flow responses behave significantly differently with different leak sizes. The pressure drop for the medium leak size is more significant than that of small size. It is observed that a small leak position at 0.75 m is difficult to locate if the pressure profile is employed as an indicator for detecting or locate leak position.

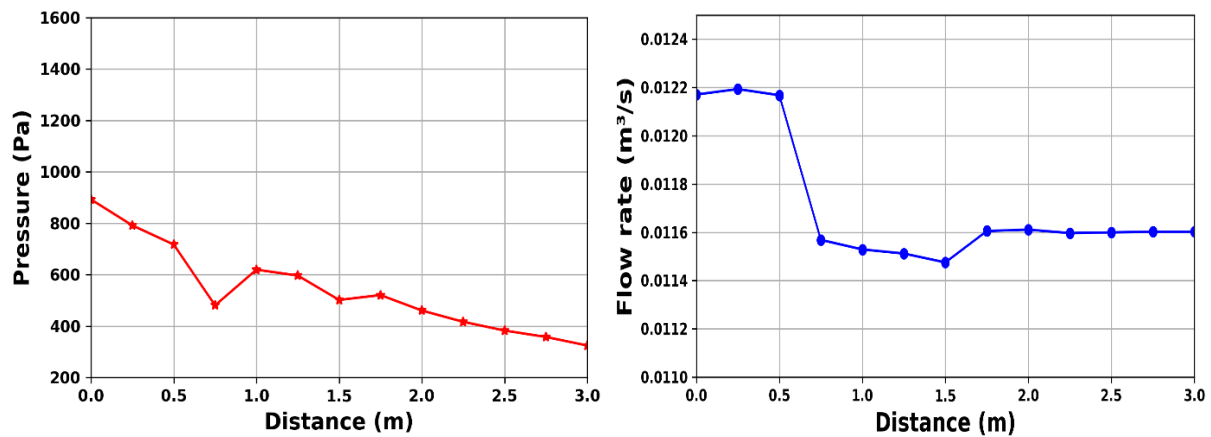
Fig. 14(b) illustrates low-medium leak scenarios with equal (medium-medium) leak sizes. The system responses show that the emergence of the second leak does not cause significant effects on the pressure drop compared to leak closer to the upstream of the pipeline. A leak closer to the pipe upstream always results in higher drop in pressure and flow rate than the second leak. Similar responses are also observed in Fig. 14(c) for the leak scenario with the large-medium leak located at 0.75 m and 1.5 m away from the upstream of the pipe, respectively. There are two major observations from the double leak scenarios: Firstly, when there are two leaks with different leak sizes, the large leak easily masks out the small one. This is because more fluid tends to escape through the large opening size. Therefore, it causes an increase in pressure drop around the large leak region. Secondly, in the event of double leaks with equal size, a leak closer to the pipe upstream has a dominant effect on the flow. This could be linked to higher pressure in the upstream section of the pipe, leading to more significant loss on the leak closer to the upstream of the pipe.



(a) low - medium sizes



(b) medium - medium sizes



(c) large - medium sizes

Fig. 14. Effect of double leaks with different leak sizes. Pressure distributions (left) and flow rate (right)).

6. Summary and conclusions

This paper presents a comprehensive simulation and assessment of multiphase flow behaviours induced by leaks in a subsea pipeline. A 3D CFD model was established to simulate different scenarios in which leak(s) may occur in subsea pipeline conveying more than one phase at a time. The VOF model and SST $k-\omega$ turbulence modelling scheme were applied to simulate the gas-liquid stratified flow in a horizontal subsea pipeline with a diameter of 60 mm. The superficial inlet velocities were chosen such that the stratified flow regime was formed. The simulation results were validated by comparing CFD results with simulation and experimental data found in the literature. The effect of leak sizes, longitudinal leak locations, multiple leakages and axial leak positions were analysed in terms of pressure gradient, flow rate and volume fractions of the gas and liquid phases. The simulation results showed that numerical simulation could help compile a set of guidelines for conducting prior leak assessment and contingency planning of accidental leakage of subsea pipeline.

It was found that when a pipeline leakage occurs, the fluids flow parameters experienced a fluctuation, particularly within the vicinity of the leak regions, which makes it possible to detect and locate the leak position. Leak size has a significant impact on the amount of fluids discharged through the leak region, which increases with the leak size. The flow parameters investigated as possible leak detection and localisation indicators are pressure drop, flow rate and volume fractions. In all cases studied, it was observed that the outlet flow rate is better for leak detection if the flow transducer is considered as an indicator for pipeline leak detection. However, upstream pressure is preferred if the pressure transducer is used as a pipeline leak detection sensor. The volume fractions are believed to be effective for quantifying the leak sizes

in the multiphase flow system. Overall, the detection of pipeline leakage appears to be easier if the pipe opening size is large and located closer to the pipe upstream. However, the impact of the leak on flow parameters is less significant when the size of the leak is small and closer to the pipeline outlet. The influence of multiple leakages on a single pipeline is investigated in different with different hole sizes, which show that effect of the leak in the region closer to the inlet of the pipeline is more significant than the second leak. Conversely, when double leaks with different sizes occur, a leak with large size is more detectable than the other.

The emphasis of this paper is to investigate the impact of leaks on two-phase gas-liquid flow behaviours and its consequences in different leak scenarios to improve the understanding of the leak effect on a multiphase subsea pipeline. The modelling and assessment presented in this study can be useful for risk assessment and improve the emergency management level. Therefore, reduce the rate of failure through early detection and localisation of pipeline leakage. The scope of this study is limited to the modelling of pipeline leakage using a CFD-based approach. Nevertheless, some areas can be further investigated in future, such as incorporating effects of temperature, gas compressibility, inlet gas volume fraction, inlet pressure and flow rate. The potential synergy of Internet of Things (IoT), digital twins and artificial intelligence (AI) technology which is expected to achieve real-time and dynamic monitoring as assessment, early notification and decision making for subsea pipeline leak detection, can be explored in the future.

Acknowledgement

The authors acknowledge the support of the Petroleum Technology Development Fund (PTDF), Abuja Nigeria, for providing funding to MAA under its Overseas Scholarship scheme.

714 **Appendix A. Nomenclature**

A	Interface area density
ANOVA	Analysis of Variance
B	Damping factor
CFD	Computational Fluid Dynamics
CSF	Continuum Surface Force
\vec{F}	Surface tension force
\vec{g}	Gravity acceleration force, m/s^2
HRIC	High-resolution interface capturing
IOGP	International Association of Oil and Gas Producers
I	Unit tensor
k	Turbulence kinetic energy, m^2/s^2
MAD	Mean Absolute Deviation
p	pressure
RANS	Reynolds-Averaged Navier-Stokes
SST	Shear Stress Transport Model
S_{ij}	average strain rate
S_ω	source term
t	time, s
VOF	Volume of Fluid
\vec{v}	velocity vector, m/s
\vec{v}^T	Transpose of the velocity vector, m/s
ω	Specific dissipation rate, $1/s$
x	Pipe length
1-D	One-dimensional
3-D	Three-dimensional

Greek symbols

ρ	density of fluid
∇	Gradient operator
$\bar{\tau}$	molecular stress tensor
$\bar{\tau}_t$	turbulent stress tensor
μ	viscosity
μ_t	dynamics viscosity
α_1	volume fractions of the secondary phase
α_2	volume fractions of the secondary phase
β	turbulence model constant
D_ω^+	dimensionless specific dissipation rate
α	Alpha

716

717 **References**

- 718 Adegboye, M.A., Fung, W.-K., Karnik, A., 2019. Recent advances in pipeline monitoring and
719 oil leakage detection technologies: principles and approaches. *Sensors*, 19(11), 2548.
720 <https://doi.org/10.3390/s19112548>.
- 721 Ajao, L., Adedokun, E., Nwishieyi, C., Adegboye, M., Agajo, J., Kolo, J., 2018. An anti-theft oil
722 pipeline vandalism detection: embedded system development. *Intern. J. of Eng. Sci. and*
723 *Applica.* 2(2), 55-64. <https://dergipark.org.tr/en/pub/ijesa/38052/408770>.
- 724 Akhlaghi, M., Mohammadi, V., Nouri, N. M., Taherkhani, M., Karimi, M., 2019. Multi-Fluid
725 VoF model assessment to simulate the horizontal air–water intermittent flow. *Chem. Eng.*
726 *Res. and Design*, 152, 48-59. <https://doi.org/10.1016/j.cherd.2019.09.031>.
- 727 Alghurabi, A., Mohyaldinn, M., Jufar, S., Younis, O., Abduljabbar, A., Azuwan, M., 2021. CFD
728 numerical simulation of standalone sand screen erosion due to gas-sand flow. *J. of Nat. Gas*
729 *Sci. and Eng.* 85, 1-15. <https://doi.org/10.1016/j.jngse.2020.103706>.
- 730 Ali, I.T., 2017. CFD prediction of stratified and intermittent gas-liquid two-phase turbulent pipe
731 flow using RANS models, PhD thesis, Faculty of Science and Engineering. The University of
732 Manchester, United Kingdom.
- 733 Ali, J.M., Hoang, N.H., Hussain, M.A., Dochainc, D., 2015. Review and classification of recent
734 observers applied in chemical process systems. *Com. & Chem. Eng.* 76, 27-41.
735 <https://doi.org/10.1016/j.compchemeng.2015.01.019>.
- 736 ANSYS, 2017. Ansys Fluent 18.1 Users Guide. ANSYS, Canonsburg, PA.

737 Araújo, M.V., Neto, S.R., Lima, A.G. B., 2013. Theoretical evaluation of two-phase flow in a
738 horizontal duct with leaks. *Adv. in Chem. Eng. and Sci.* 3, 6-14.
739 <http://dx.doi.org/10.4236/aces.2013.34A1002>.

740 Araújo, M.V., Neto, S.R., Lima, A.G.B., de Luna, F.D.T., 2014. Hydrodynamic study of oil
741 leakage in pipeline via CFD. *Adv. in Mech. Eng.* 6, 170178.
742 <https://doi.org/10.1155/2014/170178>.

743 Behari, N., Sheriff, M. Z., Rahman, M. A., Nounou, M., Hassan, I., Nounou, H., 2020. Chronic
744 leak detection for single and multiphase flow: A critical review on onshore and offshore
745 subsea and arctic conditions. *J. of Nat. Gas Sci. and Eng.*, 103460.
746 <https://doi.org/10.1016/j.jngse.2020.103460>.

747 Ben-Mansour, R., Habib, M.A., Khalifa, A., Youcef-Toumi, K., Chatzigeorgiou, D., 2012.
748 Computational fluid dynamic simulation of small leaks in water pipelines for direct leak
749 pressure transduction. *Computer & Fluids.* 57, 110-123.
750 <https://doi.org/10.1016/j.compfluid.2011.12.016>.

751 bin Md Akib, A., bin Saad, N. Asirvadam, V., 2011. Pressure point analysis for early detection
752 system. In *IEEE 7th International Colloquium on Signal Processing and its Applications*,
753 Penang, Malaysia, 4-6 March 2011. DOI: 10.1109/CSPA.2011.5759852.

754 Brackbill, J. U., Kothe, D. B., Zemach, C., 1992. A continuum method for modeling surface
755 tension. *J. of Comp. Phy.* 100, 335-354. [https://doi.org/10.1016/0021-9991\(92\)90240-Y](https://doi.org/10.1016/0021-9991(92)90240-Y).

756 Chen, L., Jin, P., Yang, J., Li, Y., Song, Y., 2021. Robust Kalman filter-based dynamic state
757 estimation of natural gas pipeline networks. *Math. Prob. in Eng.* 2021, 1-10.
758 <https://doi.org/10.1155/2021/5590572>.

759 Chen, Q., Shen, G., Jiang, J.C., Diao, X., Wang, Z. Ni, L., Dou, Z., 2018. Effect of rubber
760 washers on leak location for assembled pressurised liquid pipeline based on negative pressure
761 wave method. *Pro. Safety and Env. Prot.* 119, 181-190.
762 <https://doi.org/10.1016/j.psep.2018.07.023>.

763 Chinello, G., Ayati, A.A., McGlinchey, D., Ooms, G., Henkes, R., 2019. Comparison of
764 computational fluid dynamics simulations and experiments for stratified air-water flows in
765 Pipes. *J. of Fluids Eng.* 141(5), 051302. <https://doi.org/10.1115/1.4041667>.

766 Cramer, R., Shaw, D., Tulalian, R., Angelo, P., van Stuijvenberg, M., 2015. Detecting and
767 correcting pipeline leaks before they become a big problem. *Marine Tech. Soc. J.* 49(1), 31-
768 46. <https://doi.org/10.4031/MTSJ.49.1.1>.

769 Datta, S., Sarkar, S., 2016. A review on different pipeline fault detection methods. *J. of Loss*
770 *Prev. in the Proc. Indus.*, 41, 97-106. <https://doi.org/10.1016/j.jlp.2016.03.010>.

771 Dasgupta, S., 2016. Shell spill 88,200 gallons of oil into Gulf of Mexico.
772 <https://news.mongabay.com/2016/05/shell-spills-90000-gallons-crude-oil-gulf-mexico/>
773 (accessed 20 June 2019).

774 De Sousa, C.A., Romero, O.J., 2017. Influence of oil leakage in the pressure and flow rate
775 behaviors in pipeline. *Latin American J. of Energy Res.* 4(1), 17-29.
776 <https://doi.org/10.21712/lajer.2017.v4.n1.p17-29>.

777 Elaoud, S., Hadj-Taïeb, L. Hadj-Taïeb, E., 2010. Leak detection of hydrogen–natural gas
778 mixtures in pipes using the characteristics method of specified time intervals. *J. of Loss*
779 *Preve. in the Pro. Indus.* 23(5), 637-645. <https://doi.org/10.1016/j.jlp.2010.06.015>.

780 Espedal, M., 1998. An experimental investigation of stratified two-phase pipe flow at small
781 inclinations. PhD thesis, in: Department of Applied Mechanics, Thermo-and Fluid Dynamics.
782 Norwegian University of Science and Technology (NTNU), Norway.

783 Fu, H., Yang, L., Liang, H., Wang, S., Ling, K., 2020. Diagnosis of the single leakage in the
784 fluid pipeline through experimental study and CFD simulation. *Journal of Petroleum Science*
785 *and Engineering*, 193, 107437. <https://doi.org/10.1016/j.petrol.2020.107437>.

786 Figueiredo, A.B., Sondermann, C.N., Patricio, R.A., Bodstein, G.C., Rachid, F.B., 2017. A leak
787 localization model for gas-liquid two-phase flows in nearly horizontal pipelines. Paper
788 presented at the ASME International Mechanical Engineering Congress and Exposition, (pp.
789 1-10), Tampa, Florida, USA. <https://doi.org/10.1115/IMECE2017-71512>.

790 Guerriero, M., Wheeler, F., Koste, G., Dekate, S., Choudhury, N., 2016. Bayesian data fusion for
791 pipeline leak detection. Paper presented at the 2016 19th International Conference on
792 Information Fusion (FUSION). Heidelberg, Germany, July 5-8 2016.

793 Ijaola, A. O., Farayibi, P. K., Asmatulu, E., 2020. Superhydrophobic coatings for steel pipeline
794 protection in oil and gas industries: a comprehensive review. *J. of Nat. Gas Sci. and Eng.*
795 83(2020) 103544. <https://doi.org/10.1016/j.jngse.2020.103544>.

796 Joling, D., 2017. Alaska underwater pipeline leak may have started in December; 2017.
797 <https://apnews.com/81cc24dd5195459497f1be530d5bdb56> (access 21 March 2019).

798 Kam, S.I., 2010. Mechanistic modeling of pipeline leak detection at fixed inlet rate. *J. of Petrol.*
799 *Sci. and Eng.* 70(4), 145-156. <https://doi.org/10.1016/j.petrol.2009.09.008>.

800 Kanin, E. A., Osipov, A. A., Vainshtein, A. L., Burnaev, E. V., 2019. A predictive model for
801 steady-state multiphase pipe flow: Machine learning on lab data. *J. of Petrol. Sci. and Eng.*
802 180(2019), 727-746. <https://doi.org/10.1016/j.petrol.2019.05.055>.

803 Karim, M.Z.A., Alrasheedy, A., Gaafar, A., 2015. Compensated mass balance method for oil
 804 pipeline leakage detection using SCADA. *Int. J. Comput. Sci. Secur. (IJCSS)*, 9, 293-302.

805 Kazeem, B. A., Yskandar, H., Bolanle, T. A., Adnan, M. A., 2017. Towards achieving a reliable
 806 leakage detection and localisation algorithm for application in water piping networks: An
 807 overview. *IEEE Access*, 5, 20272-20285. DOI: 10.1109/ACCESS.2017.2752802.

808 Lazhar, A., Hadj-Taïeb, L., Hadj-Taïeb, E., 2013. Two leaks detection in viscoelastic pipeline
 809 systems by means of transient. *J. of Loss Prevent. in the Pro. Industr.* 26(6), 1341-1351.
 810 <https://doi.org/10.1016/j.jlp.2013.08.007>.

811 Li, X., Chen, G., Zheng, R., Zhu, H., Fu, J., 2018. Simulation and assessment of underwater gas
 812 release and dispersion from subsea gas pipelines leak. *Pro. Safety and Env. Protec.* 119, 46-
 813 57. <https://doi.org/10.1016/j.psep.2018.07.015>.

814 Li, X., Chen, G., Khan, F., Xu, C., 2019a. Dynamic risk assessment of subsea pipelines leak
 815 using precursor data. *Ocean Engineering.* 178, 156-169.
 816 <https://doi.org/10.1016/j.oceaneng.2019.02.009>.

817 Li, X., Chen, G., Zhu, H., 2017. Modelling and assessment of accidental oil release from
 818 damaged subsea pipelines. *Marine pollution bulletin*, 123(1-2), 133-141.
 819 <https://doi.org/10.1016/j.marpolbul.2017.09.004>.

820 Li, X., Chen, G., Zhang, R., Zhu, H., Xu, C., 2019b. Simulation and assessment of gas dispersion
 821 above sea from a subsea release: A CFD-based approach. *Intern. J. of Naval Arch. and Ocean*
 822 *Eng.* 11(1), 353-363. <https://doi.org/10.1016/j.ijnaoe.2018.07.002>.

823 Liu, C., Li, Y., Xu, M., 2019. An integrated detection and location model for leakages in liquid
 824 pipelines. *J. of Petrol. Sci. and Eng.* 175, 852-867.
 825 <https://doi.org/10.1016/j.petrol.2018.12.078>.

826 Lo, S., Tomasello, A., 2010. Recent progress in CFD modelling of multiphase flow in horizontal
827 and near-horizontal pipes. In 7th North American Conference on Multiphase Technology.
828 BHR Group, Banff, Canada, June 02, 2010.

829 Mohammed, A. I., Oyenehin, B., Atchison, B., Njuguna, J., 2019. Casing structural integrity and
830 failure modes in a range of well types-a review. J. of Nat. Gas Sci. and Eng. 68(2019),
831 102898. <https://doi.org/10.1016/j.jngse.2019.05.011>.

832 Molina-Espinosa, L., Cazarez-Candia, O. Verde-Rodarte, C., 2013. Modeling of incompressible
833 flow in short pipes with leaks. J. of Petrol. Sci. and Eng. 109, 38-44.
834 <https://doi.org/10.1016/j.petrol.2013.08.007>.

835 Movley, C., 2005. Pipeline corrosion from induced AC. In Corrosion 2005, Houston, Texas,
836 April 2005. OnePetro.

837 Bolotina, I., Borikov, V., Ivanova, V., Mertins, K., Uchaikin, S., 2018. Application of phased
838 antenna arrays for pipeline leak detection. J. of Petrol. Sci. and Eng., 161, 497-505.
839 <https://doi.org/10.1016/j.petrol.2017.10.059>.

840 Muggleton, J. M., Hunt, R., Rustighi, E., Lees, G., Pearce, A., 2020. Gas pipeline leak noise
841 measurements using optical fibre distributed acoustic sensing. J. of Nat. Gas Sci. and Eng.
842 78, 1-12. <https://doi.org/10.1016/j.jngse.2020.103293>.

843 Ranawat, N. S., Nandwana, B. P., 2021. Study of the effect of leak location in water pipeline
844 using CFD. In Recent Advances in Mechanical Engineering (pp. 173-181). Springer,
845 Singapore. https://doi.org/10.1007/978-981-15-8704-7_21.

846 Saeedipour, M., Vincent, S., Pirker, S., 2019. Large eddy simulation of turbulent interfacial
847 flows using Approximate Deconvolution Model. International J. of Mul. Flow, 1(112), 286-
848 299. <https://doi.org/10.1016/j.ijmultiphaseflow.2018.10.011>.

849 Scott, R. P., 2018. Should we call the neighbors? Voluntary deliberation and citizen complaints
850 about oil and gas drilling. *Energy Policy*. 115, 258-272.
851 <https://doi.org/10.1016/j.enpol.2018.01.017>.

852 Scott, R. P., Scott, T. A., 2019. Investing in collaboration for safety: Assessing grants to states
853 for oil and gas distribution pipeline safety program enhancement. *Energy Policy*, 124, 332-
854 345. <https://doi.org/10.1016/j.enpol.2018.10.007>.

855 Singh, J.P., Kumar, S., Mohapatra, S., 2017. Modelling of two phase solid-liquid flow in
856 horizontal pipe using computational fluid dynamics technique. *Intern. J. of Hyd. Energy*,
857 42(31), 20133-20137. <https://doi.org/10.1016/j.ijhydene.2017.06.060>.

858 Strand, O., 1993. An experimental investigation of stratified two-phase flow in horizontal pipes,
859 PhD thesis, University of Oslo, Oslo, Norway.

860 Sun, Y., Cao, X. Liang, F., 2019. Investigation on underwater spreading characteristics and
861 migration law of oil leakage from damaged submarine pipelines. *Pro. Safety. and Env. Pro.*
862 127, 329-347. <https://doi.org/10.1016/j.psep.2019.05.030>.

863 Syed, M. M., Lemma, T. A., Vandrangi, S. K., Ofei, T. N., 2020. Recent developments in model-
864 based Fault detection and diagnostics of gas pipelines under transient conditions. *J. of Nat.*
865 *Gas Sci. and Eng.* 83, 1-21. <https://doi.org/10.1016/j.jngse.2020.103550>.

866 Wang, X., Ghidaoui, M. S., 2018. Pipeline leak detection using the matched-field processing
867 method. *J. of Hydraulic Eng.* 144(6), 04018030. [https://doi.org/10.1061/\(ASCE\)HY.1943-](https://doi.org/10.1061/(ASCE)HY.1943-7900.0001476)
868 [7900.0001476](https://doi.org/10.1061/(ASCE)HY.1943-7900.0001476).

869 Wang, X., Tan, Y., Zhang, T., Xiao, R., Yu, K., Zhang, J., 2021. Numerical study on the
870 diffusion process of pinhole leakage of natural gas from underground pipelines to the soil. *J.*
871 *of Nat. Gas Sci. and Eng.* 87, 1-14. <https://doi.org/10.1016/j.jngse.2020.103792>.

872 Wei, O.Y., Masuri, S.U., 2019. Computational fluid dynamics analysis on single leak and double
873 leaks subsea pipeline leakage. *CFD Letters*, 11, 95-107.

874 Yang, Z., Fan, S., Xiong, T., 2010. July. Simulation and numerical calculation on pipeline
875 leakage process. *IEEE 2nd International Symposium on Information Engineering and*
876 *Electronic Commerce*, Ternopil, Ukraine, July 23-25 2010. DOI:
877 10.1109/IEEC.2010.5533189.

878 Zhu, H., Lin, P., Pan, Q., 2014. A CFD (computational fluid dynamic) simulation for oil leakage
879 from damaged submarine pipeline. *Energy*, 64, 887-899.
880 <https://doi.org/10.1016/j.energy.2013.10.037>.